Reanalysis of Uranus' cloud scattering properties from IRTF/SpeX observations using a self-consistent scattering cloud retrieval scheme.

P.G.J. Irwin[a], D.S. Tice[a], L.N. Fletcher[a], J.K. Barstow[a], N.A. Teanby[b], G.S. Orton[c], and G.R. Davis[d].

[a]Atmospheric, Oceanic, and Planetary Physics, Department of Physics, University of Oxford, Clarendon Laboratory, Parks Road, Oxford, OX1 3PU, United Kingdom.

Tel: (+44) 1865 272933, *Fax:* (+44) 1865 272923. E-mail: irwin@atm.ox.ac.uk

[b]School of Earth Sciences, University of Bristol, Wills Memorial Building, Queen's Road, Bristol, BS8 1RJ, United Kingdom.

[c]Jet Propulsion Laboratory, California Institute of Technology, 4800 Oak Grove Drive, Pasadena, CA 91109, USA.

[d]Joint Astronomy Centre, 660 N. A'ohoku Place, Hilo, Hawaii HI 96720, USA.

Original: 17/10/14: Revised 5/12/14

Number of manuscript pages: 28 + acknowledgements, references, figure legends and tables (52 in total).

Number of Figures: 14

Number of Tables: 5

Proposed running head:

Uranus Near-IR Cloud Scattering Properties

Editorial correspondence should be directed to:

Prof. Patrick G. J. Irwin,

Atmospheric, Oceanic and Planetary Physics, Clarendon Laboratory, Parks Road,

Oxford OX1 3PU, United Kingdom.

Telephone: (+44) 1865 272933 (direct line: 272083)

Fax: (+44) 1865 272923

Email: irwin@atm.ox.ac.uk

Abstract

We have developed a new retrieval approach to modelling near-infrared spectra of Uranus that represents a significant improvement over previous modelling methods. We reanalysed IRTF/SpeX observations of Uranus observed in 2009 covering the wavelength range 0.8 – 1.8 μm and reported by Tice et al. (2013). By retrieving the imaginary refractive index spectra of cloud particles we are able to consistently define the real part of the refractive index spectra, through a Kramers-Kronig analysis, and thus determine self-consistent extinction cross-section, single scattering and phase-function spectra for the clouds and hazes in Uranus' atmosphere. We tested two different cloud-modelling schemes used in conjunction with the temperature/methane profile of Baines et al. (1995), a reanalysis of the Voyager-2 radio-occultation observations performed by Sromovsky, Fry and Tomasko (2011), and a recent determination from Spitzer (Orton et al., 2014). We find that both cloud-modelling schemes represent the observed centre-of-disc spectrum of Uranus well, and both require similar cloud scattering properties of the main cloud residing at ~2 bars. However, a modified version of the Sromovsky, Fry and Tomasko (2011) model, with revised spectral properties of the lowest cloud layer, fits slightly better at shorter wavelengths and is more consistent with the expected vertical position of Uranus' methane cloud.

We find that the bulk of the reflected radiance from Uranus arises from a thick cloud at approximately the 2 bar level, composed of particles that are significantly more absorbing at wavelengths $\lambda > 1.0$ μm than they are at shorter wavelengths $\lambda <$ 1.0 μm. This spectral information provides a possible constraint on the identity of the main particle type, although we find that the scattering properties required are not consistent with any of the available laboratory data for pure NH_3, NH_4SH, or CH_4 ice

(all suspected of condensing in the upper troposphere). It is possible that the observed clouds are mixtures of tropospheric condensate mixed with photochemical products diffusing down from above, which masks their pure scattering features. Because there is no available laboratory data for pure H_2S or PH_3 ice (both of which might be present as well), they cannot be excluded as the cloud-forming species. We note, however, that their absorptive properties would have to be two orders of magnitude greater than the other measured ices to be consistent with our retrieval, which suggests that mixing with photochemical products may still be important.

1. Introduction

The visible/near-infrared spectrum of Uranus is formed by reflection of sunlight from various levels in the planet's atmosphere that are modulated by the transmission of methane gas, H_2-H_2 (collision-induced absorption) and Rayleigh scattering. It thus provides unique constraints on Uranus' vertical cloud structure and also on the scattering properties of Uranus' hazes and condensates. Many observations of Uranus' near-IR spectrum have been made in the last decade, through Uranus' northern spring equinox in 2007. A number of modelling studies have attempted to interpret these data, including Baines and Bergstrahl (1986) (0.35-1.05 μm), Pollack et al. (1987) (0.43 – 0.6 μm), Rages et al. (1991) (Voyager 2: 0.35 – 0.62 μm), Karkoschka and Tomasko (2009) (HST/STIS: 0.3-1.0 μm), Sromovsky, Irwin and Fry (2006), Sromovsky and Fry (2006, 2008), Sromovsky, Fry and Kim (2011) and Irwin et al. (2007, 2009, 2010, 2011, 2012a,b) (1.2-1.8 μm). One of the primary results of these studies is that the abundance of methane in the upper troposphere of Uranus varies with latitude (Karkoschka and Tomasko, 2009). Since we use methane absorption features to probe the vertical level of the clouds this means that the

84 determined cloud levels are unreliable unless this methane variation is accounted for.
85 Fortunately, this degeneracy can be broken at a few places in Uranus' spectrum, most
86 easily at 0.825 μm (Karkoschka and Tomasko, 2009), where a collision-induced-
87 absorption band of H_2-H_2 is found. However, the degeneracy can also be broken in
88 the H-band (1.4 – 1.8 μm) if the spectrum is observed at sufficiently high spectral
89 resolution (Irwin et al., 2012b). Most recently, Tice et al. (2013) analysed IRTF/SpeX
90 observations of Uranus made in 2009 and attempted to determine cloud parameters
91 that could be applied over the entire SpeX range of 0.8-1.8 μm using both compact
92 and vertically extended clouds/hazes. Tice et al. (2013) found a variation of methane
93 abundance with latitude that was consistent with Karkoschka and Tomasko (2009),
94 but also found that the particles in the main cloud deck at 2-3 bars must be
95 significantly more absorbing at longer wavelengths with the single scattering albedo
96 varying from 1.0 for $\lambda < 1.0$ μm to 0.7 for wavelengths longer than 1.4 μm, a
97 conclusion previously reached from UKIRT/UIST observations by Irwin, Teanby and
98 Davis (2010). In this paper we attempt to reconcile the conclusions of Tice et al.
99 (2013) with that of a reanalysis of HST/STIS observations by Sromovsky, Fry and
100 Kim (2011), who approached the problem from the perspective of first determining a
101 vertical profile of methane (and H_2, He and Ne) that was consistent with both the
102 Voyager 2 radio-occultation observations (Lindal et al. 1987) and also cloud and haze
103 vertical distributions inferred from observations in the visible and near-IR.
104 Since the identity of Uranus' cloud particle types is not unambiguously known,
105 previous attempts to model the cloud scattering properties have used empirically
106 adjusted scattering properties, such as assuming extinction cross-section and phase-
107 function spectra, or empirically adjusting the phase function. Although simple, these
108 techniques are rather unphysical and also have usually only been applied to narrow

wavelength ranges, making it difficult to match the derived quantities with the laboratory-measured spectra of candidate condensates. In this paper we present a new retrieval scheme that returns a physically based self-consistent determination of the scattering properties of Uranus' clouds. This approach can be applied simultaneously over a wide spectral range and the retrieved cloud parameters can be easily compared with the measured properties of candidate condensates. Section 2 descibes our new retrieval scheme and applies it to the IRTF/SpeX observations (0.8-1.8 μm) presented by Tice et al. (2013), using their simple 2-cloud model. We also assess the effects on these retrievals of using the temperature-abundance profiles derived from Spitzer (Orton et al., 2014) and the 'F1' profile of Sromovsky Fry and Kim (2011). Section 3 then compares the observed IRTF/SpeX observations with the predictions of the 5-cloud model and revised temperature-abundance profiles of Sromovsky, Fry and Kim (2011). Section 4 applies our new retrieval scheme to fitting the IRTF/SpeX spectra with a revised model based on the Sromovsky, Fry and Kim (2011) scheme, while section 5 presents a discussion of the derived scattering properties retrieved. Section 6 summarises our conclusions.

2. Reanalysis of IRTF spectra with a simple two-cloud model

Tice et al. (2013) (henceforth T2013) analysed SpeX long-slit spectra of Uranus, recorded in 2009 at NASA's Infrared Telescope Facility (IRTF) on Mauna Kea, Hawaii. The slit was aligned with Uranus' central meridian and spectra recorded from 0.8 to 1.8 μm with a spectral resolution of 1200 and with an average 'seeing' that varied from 0.5" in the H-band (1.4-1.8 μm) to 0.6" in the I-band (0.8-0.9 μm). Together with a thin extended haze above the 1-bar pressure level, the main cloud deck in Uranus' atmosphere is found by numerous studies to reside in the 2-3 bar

pressure region and is of unknown composition, although from thermochemical models is expected to be formed of H_2S or possibly NH_3 ice. Since the precise identification is unknown, and spectroscopic information for condensates such as H_2S is not available, it is necessary to make some assumptions on the particles' scattering properties and different authors have adopted different approaches for how to do this. For example, T2013 assumed that the particles in the main cloud deck and in the haze had the same phase function at all wavelengths (parameterised with a Henyey-Greenstein phase function with an asymmetry parameter g = 0.7) and set the variation of extinction cross-section with wavelength using Mie theory (e.g. Hansen and Travis, 1971) for particles with a complex refractive index of 1.4+0i at all wavelengths and different particle size distributions (a standard Gamma size-distribution was assumed, where $n(r) \propto r^{(1-3b)/b} e^{-r/ab}$, a is the mean radius and b the variance). The single-scattering albedo spectrum was then adjusted empirically at different wavelengths to improve the fit between the measured and synthetic spectra. Other authors, such as Sromovsky, Fry and Kim (2011) (henceforth SFK2011), empirically adjusted the phase function and/or single scattering albedo as a function of wavelength. We shall return to the approach of SFK2011 later in this paper.

While providing a reasonable starting point for analysing Uranus spectra, the method of T2013, which is based on earlier work by Irwin et al. (2010, 2011, 2012a), is less applicable to data such as IRTF/SpeX that cover a large wavelength range than to small individual wavelength ranges, for which the technique was originally developed. In reality, we expect the phase function to vary with wavelength. Furthermore, it is not very realistic to model the haze, composed of very small particles, with the same phase function as that used for the main cloud deck, composed of micron-sized particles, since small particles would be expected to

158 behave more like Rayleigh scatterers. It is also not very consistent to set the extinction
159 cross-section spectrum equal to that for Mie particles with a single conservative
160 refractive index at all wavelengths and then adjust the single scattering albedo
161 independently. Thus, in this paper we set out to improve the physical plausibilty of
162 our cloud retrievals by representing the clouds in a more self-consistent manner such
163 that the phase functions used at different wavelengths are consistent with the cross-
164 section and single-scattering albedos. In order to construct this more self-consistent
165 model we needed to define at a more fundamental level the scattering properties of
166 the particles.

167 For Uranus' clouds we expect there to be some variation of single-scattering
168 albedo, cross-section and phase function with wavelength. However, instead of
169 varying each of these individually, we chose instead to represent this by varying the
170 imaginary part of the particles' complex refractive spectrum. Given the imaginary
171 part of a particle's refractive index spectrum, n_i, we can determine the real part, n_r,
172 using the Kramers-Kronig analysis (e.g. Sheik-Bahae, 2005), providing we know the
173 value of the real part of the refractive index spectrum at some reference wavelength.
174 We know from laboratory studies that the real part of the refractive index for most
175 particles that may condense in outer planet atmospheres is between 1.3 and 1.4. For
176 example, Martonchik, Orton and Appleby (1984) quote n_r = 1.408 for ammonia ice at
177 1.46 μm and Martonchik and Orton (1994) quote a value n_r =1.311 for methane ice at
178 the same wavelength. Hence, in this paper we fixed the real part of the refractive
179 index to be nominally 1.4 at an arbitrary reference wavelength, usually 1.4 μm, and
180 determined the value at other wavelengths from the fitted imaginary refractive index
181 spectrum via a Kramers-Kronig analysis. Note that we also made test retrievals for
182 other choices of the fixed real refractive index value, which we report later. We would

still expect there to be a distribution of particle sizes and so we chose to continue to represent the size distribution with standard Gamma distributions with mean radius and variance. Using the complex refractive index spectrum together with this particle size distribution, standard Mie theory (e.g. Hansen and Travis, 1974) may be used to calulate self-consistent extinction cross-section, single-scattering albedo and phase-function spectra, which can then be used in a radiative transfer model to test against the observed spectra. Hence, by assuming the real part of the refractive index at a single wavelength and fitting the imaginary part of the refractive index spectrum and the parameters of the particle size-distribution, all the other scattering parameters can be calculated completely self-consistently.

We thus added a new parameterisation scheme to our NEMESIS (Irwin et al. 2008) retrieval model, where for each haze or cloud particle type we retrieve the mean radius and variance of the standard Gamma particle-size distribition together with the imaginary refractive index spectrum over the wavelength range of interest. At each iteration NEMESIS takes the latest retrieved values of these parameters, computes the real part of the refractive index spectrum using the Kramers-Kronig analysis and calculates the extinction cross-section, single-scattering albedo and phase-function spectra using Mie theory. NEMESIS then uses these parameters in its existing multiple-scattering model to simulate the observed Uranus IRTF/Spex spectra, although the Mie-scattering calculated phase functions were first approximated with combined Henyey-Greenstein functions to smooth over some features in these phase functions peculiar to purely spherical particles, such as the 'rainbow'. While we would not expect the mean radius and variance to be correlated with any other parameter, we might reasonably expect that the imaginary refractive index spectrum should be a smoothly varying function of wavelength. This smoothing was applied via

208 a correlation length in the *a priori* covariance matrix with off-diagonal elements set as
209 $S_{ij} = \left(S_{ii}S_{ij}\right)^{1/2}\exp\left((\lambda_i - \lambda_i)/c\right)$, where c is a 'correlation length' (which was set to
210 0.1 μm, to provide wavelength-smoothing on a scale consistent with the laboratory
211 spectra of candidate condensates, shown later in Fig. 14) and λ_i is the wavelength of
212 the i^{th} refractive index.

213 While our previous approach of using *ad hoc* cross-section, single-scattering, and
214 Henyey-Greenstein phase-function spectra allowed us great flexibilty in providing
215 plenty of parameters to adjust in order to minimise the closeness of fit between the
216 observed and modelled spectra, this new system has fewer free parameters, but
217 returns a solution that is self-consistent. However, it has to be assumed that the
218 particles can be well modelled with Mie theory. Whilst this is certainly true for
219 spherical droplets, Mie theory is less applicable to solid particle scatterers, such as
220 methane, H_2S and NH_3 ice, whose crystals will not be spherical. However, if we
221 assume the ice particles are randomly oriented with respect to each other, then the
222 Mie approach provides a first-order approximation, although a set of Mie scatterers
223 exibit peaks at angles related to the 'rainbow' and also a higher back-scattering peak
224 (the 'glory'), which are features that are absent from a distribution of non-spherical
225 particles. However, such features are smoothed by our approach of using combined
226 Henyey-Greenstein approximations to the calculated phase functions and our
227 technique of retrieving the imaginary refractive index greatly helps to limit the range
228 of solutions to ones more likely to be physically plausible. We will return to the
229 applicability of the Mie approach in the discussion section and outline possible future
230 refinements there.

231 To assess the new retrieval scheme we initially adopted the same model as
232 T2013: namely a two-cloud model with the original reference methane profile (Baines
233 et al., 1995) used by Irwin et al. (2007) with a deep volume mixing ratio of 1.6%,
234 limited to 30% relative humidity in the upper troposphere and frozen to its cold trap
235 value in stratosphere. We used the same IRTF/SpeX spectra reported by T2013 and
236 fitted to the spectrum recorded closest to the equator at 1.3°S. The same Matrix-
237 Operator scattering model of Plass et al. (1973) was used, with the inclusion of
238 Rayleigh scattering by the air molecules themselves, with 5 zenith angles and N
239 Fourier components to cover the azimuth variation, where N is set adaptively from the
240 viewing zenith angle, θ, as $N = int(\theta/3)$. Methane gaseous absorption was modelled
241 with the k-coefficients of Karkoschka and Tomasko (2010) and the H_2-H_2/H_2-He CIA
242 coefficients of Borysow (1991, 1992), Zheng and Borysow (1995) and Borysow et al.
243 (2000) were employed. The contribution of clouds and aerosols was modelled with
244 two discrete clouds, each with a specified base pressure, fractional scale height
245 (relative to the atmospheric pressure scale height) and optical depth. Following on
246 from T2013 the *a priori* main Tropospheric Cloud (TC) was modelled with a base
247 pressure of 2.7 bar, fractional scale height 0.08 and opacity (at 1.6 μm) of 5.5, while
248 the Tropospheric Haze (TH) was modelled with a base pressure of 1 bar, fractional
249 scale height 0.93 and opacity (at 1.6 μm) of 0.027. All six parameters were allowed to
250 vary in these new retrievals with the exception of the haze base pressure, which was
251 fixed at 1 bar, which T2013 found to be the optimal pressure. The tropospheric cloud
252 was assumed to be composed of particles with *a priori* mean radius 1 μm, and
253 variance 0.05, while the haze particles were assumed to be composed of particles with
254 *a priori* mean radius 0.1 μm, with the same variance. The *a priori* imaginary
255 refractive index spectrum of both particles was set to (0.001±0.0005) at all

256 wavelengths, while the real part of the refractive index at 1.4 μm was set to 1.4.For
257 the forward-model calculations, the atmosphere between 17 and 0.01 bar was split
258 into 39 levels of equal thickness in log (pressure) and the cloud parameterisation
259 scheme used to determine the opacity of both cloud types in each layer.

260 The NEMESIS model was then run until it converged to the solution shown in
261 Fig. 1, where it can be seen that we have achieved a good fit to the IRTF/SpeX
262 spectra across the entire wavelength range (NB the section between 1.35 and 1.46 μm
263 has been omitted due to low S/N caused by telluric water absorption). Figure 1 also
264 shows the fit achieved to this spectrum using the original model of T2013 with
265 emprically adjusted scattering properties, together with one with the empirical T2013
266 properties, but where the assumed temperature and abundance profiles are those
267 determined to best fit Uranus Spitzer observations (Orton et al. 2014), which has a
268 deep methane volume mixing ratio of 3.2%. To achieve these fits, Fig. 2 shows the
269 fitted cloud profiles (optical depth/bar at 1.6 μm), while Fig. 3 shows the retrieved
270 complex refractive index spectra of the Tropospheric Cloud (TC) and Tropospheric
271 Haze (TH) fitted by our model for the self-consistent modelling case, together with
272 the fitted particle size-distribution parameters. These refractive indices are also listed
273 in Table 1. In our model we actually fit values of $\log(n_i)$, in order to ensure that n_i
274 never becomes negative. Our *a priori* values of n_i were 0.001±0.0005, in other words
275 a fractional error of 50% and if we plot $\log(n_i)$, as we do in Fig.3, then retrieved
276 values with the same fractional error have identically large error bars, which enables
277 the reader to see more clearly where the retrieval is giving us meaningful information.

278 For the main Tropospheric Cloud (TC) deck, we see that we require the particles
279 to become substantially absorbing at wavelengths greater than 1.0 μm and from the
280 size of the error bars we can see that this requirement is well constrained. At shorter

281 wavelengths we can see that the retrieved values of n_i are very similar to the *a priori*,
282 and the retrieved errors are only slightly smaller, suggesting we have limited
283 sensitivity. For particles in the Tropospheric Haze (TH) we find that our solution
284 barely moves from the a priori, indicating that we have little sensitivity to its
285 imaginary refractive index, presumably due to its low optical depth and this small
286 effect on the measured spectrum.

287 To assess the sensitivity of our solution to the assumed *a priori* imaginary
288 refractive index, n_i, the retrieval was repeated for *a priori* imaginary refractive indices
289 in the range 0.005, 0.01, 0.05, 0.1 (again with *a priori* errors of 50%) for both TC and
290 TH particles. The results of these retrievals (and the n_i=0.001 case) are shown
291 together in Fig. 4. Considering first the results for the Tropospheric Cloud (TC)
292 particles, we can see that the solutions all converge to increased absorption at
293 wavelengths greater than 1.0 μm. However, the solutions are by no means unique and
294 the spread of results is greater than the formal retrieval errors on individual elements
295 of the solution, which is unsurprising given the non-linearity of this retrieval approach
296 and the various cross-correlations that are absent from the formal errors on individual
297 elements. The mean and standard deviation of all five cases are also shown in Fig.4
298 and this represents a more conservative and realistic estimate of the required
299 imaginary refractive index spectrum and its variance. Furthermore, modelling
300 multiple *a priori* n_i values also allows us to determine the likely spread in the real
301 component of the real refractive index. For the Tropospheric Haze (TH) particles we
302 can see that the results do not seem to converge at all, confirming that we are not able
303 to infer meaning information on the TH n_i spectrum using this method. Figure 5
304 shows the range in extinction cross-section and single-scattering albedo solutions
305 resulting from the 5 different *a priori* n_i cases. Again, we see that the properties of the

306 TC particles are reasonably well constrained, but not those of the TH particles. It
307 should be noted that results are obtained from a single spectrum observed with near-
308 nadir conditions and thus the effect of the tropospheric haze is small. Scattering in this
309 layer will become more prominent at higher angles and it is possible that a limb-
310 darkening analysis would provide greater constraint on the haze particle
311 characteristics. However, such a study is beyond the scope of these IRTF/SpeX data,
312 which only measured Uranus along its central meridian.

313 Also plotted in the top right panel of Figs. 3 and 4 are the required imaginary
314 refractive indices necessary to produce single scattering albedoes consistent with
315 those assumed by T2013 for the TC in their empirical model. We can see that for the
316 TC we require the imaginary part of the refractive index to increase markedly for
317 wavelengths greater than 1 μm. This is necessary to lower the single-scattering albedo
318 sufficiently to reduce the reflectivity of the peaks at $\lambda > 1$ μm relative to those at $\lambda <$
319 1 μm. This adjustment to the single scattering albedo is very similar to that
320 empirically arrived at by Irwin, Teanby and Davis (2010) and later by Tice et al.
321 (2013). However, in this case we have achieved this result with a self-consistent
322 model that is more physically plausible. For the $n_i = 0.001$ case we estimate the mean
323 particle size in the Tropospheric Cloud (TC) to be 0.89 ± 0.04 μm, compared with the
324 *a priori* of 1.0 ± 0.05 μm, while in the Tropospheric Haze (TH) we derive values of
325 0.178 ± 0.013 μm, compared with the a priori of 0.1 ± 0.05 μm (similar sizes were
326 obtained with other a priori values of n_i) Hence, we see we are rather more sensitive
327 to the size of the TH particles, than we are to the size of the TC particles. However,
328 we find we are not very sensitive to the variance of the TC and TH size distributions,
329 which did not vary significantly from their a priori values of 0.05. The self-consistent
330 retrieval model is found to fit the observed IRTF/SpeX spectrum slightly better than

the emprical T2013 approach with χ^2/n=1.00, compared with χ^2/n=1.04. Since there were 442 points in the spectrum to be fitted this represents a change of $\Delta\chi^2 = 18$, which is significant. The retrieved cloud profiles, shown in Fig 2., can be seen to be very similar for the retrieved self-consistent and assumed empirical scattering parameter approaches. When using the empirical scattering parameter approach with the Spitzer temperature-abundance profile (shown in Fig. 6) we find the TC must reside at slightly lower pressures, as expected, since the deep methane abundance is higher, but we achieved a significantly poorer fit (χ^2/n=1.24).

With this method we can compare our derived refractive indices with the published refractive index spectra of candidate condensate materials to see if some candidate particles might be more consistent than others. We shall return to this point later in Section 5, but at this point we explored the extent to which our fits depended on the assumed value of the real refractive index, n_r, at our reference wavelength of 1.4 μm. We performed retrievals using different assumed real refractive index values at 1.4 μm (for both haze and cloud particles) of 1.2, 1.4, 1.7, 2.0 and 2.4, with the same imaginary refractive index of 0.001. We found that the closeness of fit did depend on n_r with fitted values of χ^2/n of 0.96, 1.00, 1.11, 1.52 and 1.37 respectively. Hence, particles with higher values of n_r seem less able to reproduce the peak radiances at lower wavelengths and thus our analysis favours solutions with lower values of n_r.

3. Consistency of IRTF/SpeX observations with HST/STIS cloud model

A major drawback of the Irwin et al. (2009-2012a) and T2013 approach was that the methane profile was fixed to be the same at all latitudes, with a deep abundance of 1.6%, after Baines et al. (1995). The main gaseous absorber in the near-IR spectrum

355 of Uranus is methane and to use these features to infer cloud top positions a volume
356 mixing ratio profile must be assumed. Although we know that methane condenses in
357 the troposphere, at wavelengths greater than 1 μm and at the lower resolutions once
358 available there was no way to discriminate between cloud top height and methane
359 abundance. Thus in the absence of any better information it was assumed that the
360 same methane profile could be used at all latitudes, allowing cloud heights to be
361 retrieved. While discrimination between methane and cloud top height is difficult at
362 wavelengths > 1 μm, it becomes less difficult at shorter wavelengths, where methane
363 absorption becomes less pronounced and the collision-induced absorption bands of
364 H_2-H_2 become more prominent. Karkoschka and Tomasko (2009) (henceforth
365 KT2009). analysed HST/STIS observations of Uranus measured in 2002 in the
366 wavelength range 0.3 – 1 μm. Analysing the absorptions around the second overtone
367 band of H_2-H_2 collision-induced absorption around 825 nm, KT2009 were able to
368 show that the tropospheric mole fraction of methane at equatorial latitudes has values
369 of ~4%, decreasing to < 2% at polar latitudes. The IRTF/SpeX observations analysed
370 by T2013 (and reanalysed here) also include this 825 nm region and T2013 were able
371 to confirm this enrichment of methane at equatorial latitudes. At longer wavelengths,
372 improved spectroscopic line parameter data allowed Irwin et al. (2012b) to reanalyse
373 Gemini/NIFS H-band observations at their native spectral resolution of R = 5370 to
374 determine that a latitudinally varying methane abundance profile was also most
375 consistent with these observations. Irwin et al. (2012b) found similar enhancements of
376 methane at equatorial latitudes.

377 In addition to the methane-abundance/cloud-height degeneracy problem, a second
378 puzzle for Uranus cloud studies has been discrepancies between the
379 temperature/pressure profile previously used for Uranus cloud retrievals and the

expected position of clouds from thermochemical considerations. The Voyager-2 radio-occultation observations of Uranus reported by Lindal et al. (1987) indicated a sudden change of density (presumed to be associated with the condensation level of methane) at about 1.2 bar, which coincides with the approximate level of observed discrete clouds, thought to be methane ice. Unfortunately, the temperature/pressure profile of the reference 'D' profile derived by Lindal et al. (1987) (and used in the Baines et al., 1995 model) is inconsistent with the thermal properties of methane ice, which in such a profile would condense at significantly higher pressures than 1.2 bars, especially for cases where the deep abundance of methane was as high as 4% as estimated by KT2009.

SFK2011 reanalysed the Voyager-2 radio-occulation profiles of Lindal et al. (1987). They determined that self-consistent temperature, pressure, and abundance profiles could be constructed with a deep methane abundance of 4% and methane cloud condensation level of ~1.2 bar if the He volume mixing ratio were reduced from 0.15 to 0.116, near the edge of the uncertainty range quoted by Conrath et al. (1987), and a small abundance of Ne (0.04%) were added. SFK2011 then went on to reanalyse the 2002 HST/STIS 0.3-1.0 μm observations of KT2009 and found that their 'F1' solution to the Voyager 2 radio-occultation data provided the best consistency with the observed spectra when used in conjunction with a vertical cloud model having five different particle types and layers with empirically determined scattering properties, building upon the model of KT2009. The 'F1' profile of SFK2011 is compared with the Baines et al. (1995) profile used by T2013 and with the Spitzer profile of Orton et al. (2014) in Fig. 6.

The different cloud layers and scattering properties of the SFK2011 cloud scheme are outlined in full in Table 2, and are based on empirical deductions and

405 approximations, similar in flavour, but different from, the assumptions made by
406 T2013. For example, for their stratospheric haze the real part of the refractive index
407 was set to 1.4 everywhere and an empirical function used for the imaginary refractive
408 index spectrum. For other particle types, an empirical single-scattering albedo
409 spectrum was imposed, together with an assumed phase function. SFK2011 applied
410 this model to the 0.3 – 1 μm HST/STIS range, but Table 2 also specifies how these
411 parameters were extended to the 1-2 μm range (Fig. 9 of SFK2011). As can be seen
412 the assumed scattering properties are empirical, but given that we do not have good
413 information on the actual particle properties in Uranus' atmosphere, such assumptions
414 are as valid as those used by T2013 and were found to be consistent with the
415 HST/STIS and previous Voyager-2 observations.

416 To assess how consistent the 'F1' temperature/pressure/methane profile and
417 cloud parameterisation scheme of SFK2011 might be with our IRTF/SpeX
418 observations from 0.8 – 1.8 μm, we added a new parameterisation scheme to
419 NEMESIS to split the atmosphere into layers that coincided with the edges of the 5
420 different cloud layers. The base pressures of the 5 cloud and haze layers were set and
421 in the case of the three tropospheric clouds the upper pressures scaled from the base
422 pressures with factors of 0.98, 0.93 and 0.93 for the Lower, Middle and Upper
423 Tropospheric clouds respectively. These three clouds were each represented by a
424 single layer in our model. The two haze layers were set to lie between 0.9 and 0.1 bar
425 for the Tropospheric Haze and between 0.1 and 0.01 bar for the Stratospheric haze.
426 The hazes were subdivided into 5 layers equally spaced in log pressure. The clear
427 atmosphere between the tropospheric clouds was split into 4 layers, with an additional
428 4 layers placed below the Lower Tropospheric Cloud, extending to a deepest pressure
429 of 12.4 bars and 4 layers placed above the top of the Statospheric Haze extending to

lowest pressure of 0.00003 bar. Except for the thin clouds, and the edges of the haze layers, which were set to specific pressure levels, all intermediate layers were equally spaced in log pressure. In all, this representation had 38 layers. Rayleigh scattering was again included.

Using this new model, the fitted opacities and pressures reported in Table 2 of SFK2011 were used to reproduce the synthetic spectra reported in their Fig. 7c. We found we were able to fully reproduce their 0.3-1.0 μm synthetic spectra with very good accuracy and also tested that our model reproduced the scattering efficiencies, single scattering albedos, backscatter phase function and backscatter efficiency shown in their Fig. 9. Having established that we were accurately reproducing the synthetic spectra of SFK2011 we then tested to see how well this model might be consistent with our IRTF/SpeX observations.

For comparison with the T2013 model, we again chose the IRTF/SpeX spectrum closest to the equator at 1.3°S, shown in Fig. 1. Figure 7 shows the agreement between our observed spectrum and the synthetic calculation using purely the SFK2011 cloud model and scattering properties. It can be seen that the SFK2011 simulates the spectrum from 0.8 – 1.1 μm very well, as we might expect, but it departs significantly from the IRTF/SpeX spectrum from 1.1 to 1.8 μm, with the radiance in the reflectance peaks and in the methane absorption bands being too high. Figure 8 shows the effect on the modelled spectrum of removing each of the five clouds in turn, where we can see that, as expected, the peak reflectivities are modulated mainly by the tropospheric clouds, while the hazes control the reflectivity in the methane absorption bands. Figure 8 shows that scattering from the upper tropospheric haze is mainly responsible for the reflection at 1.7 μm and is clearly too high. The scattering properties of this haze were modelled by SFK2011 as having a

455 wavelength-independent cross-section and empirical single-scattering albedo and
456 phase function, but these assumptions are clearly not valid in the 1 – 2 μm range.
457 Similarly, we can see that the reflection in the peaks at wavelengths greater than 1.2
458 μm needs to be less, just as was found by Irwin, Teanby and Davis (2010) and Tice et
459 al. (2013). This suggests that the tropospheric cloud reflectivities need to be lower at
460 these wavelengths, either due to lower single-scattering albedo, lower cross-section,
461 lower backscatter efficiency or a combination of all three.

462 Although not consistent without modification with the IRTF/SpeX observations,
463 the SFK2011 model has significant merit in that it has a methane cloud roughly where
464 we might expect one to be from thermochemical equilibrium for the increased deep
465 tropospheric abundance of methane at the equator (4%) determined by KT2009.
466 Hence, we tested this approach further, using their 'F1' profile in conjuction with the
467 same 5-cloud model used by SFK2011, but replacing the scattering properties of some
468 of the clouds with self-consistent scattering properties determined with NEMESIS
469 using our new scheme.

470 **4. Reanalysis of IRTF/SpeX observations using 'F1' vertical profile and 5-cloud**
471 **SFK2011 model.**

472 Using the SFK2011 5-cloud-layer scheme and their 'F1' temperature/abundance
473 profile we attempted to see how well we might be able to fit the IRTF/SpeX
474 observations. Since we found that we had little sensitivity to the pressure level of the
475 Lower Tropospheric Cloud (LTC), we fixed its location to a base pressure of 5 bars.
476 In this model the upper tropospheric cloud (UTC) is presumed to be the methane
477 cloud and hence we fixed its position to the methane condensation level for the 'F1'
478 profile of 1.23 bar. We also left the Tropospheric Haze (TH) and Stratospheric Haze

479 (SH) between their prescribed pressure limits since previous analyses of these data
480 have indicated that we have limited sensitivity to the vertical position of the haze,
481 other than requiring it to reside at pressures less than ~1 bar. We did, however, allow
482 the base pressure of the Middle Tropospheric Cloud (MTC) to vary. We left the
483 optical properties of the Lower Tropospheric Cloud (LTC), Upper Tropospheric
484 Cloud (UTC) and Stratospheric Haze (SH) to those specified by SFK2011,
485 extrapolating as they suggested to the 1 – 2 μm range, but retrieved the scattering
486 properties of the Middle Tropospheric Cloud (MTC) and Tropospheric Haze (TH)
487 using our self-consistent refractive index retrieval method, using the same set-up as
488 was used to determine the optical properties of the Tropospheric Cloud (TC) and
489 Tropospheric Haze (TH) of the 2-cloud T2013 model. The optical depths of all the
490 clouds were allowed to vary.

491 This model was then fitted to the near-centre-of-disc IRTF/SpeX observations at
492 1.3° S and the resulting fit is shown in Fig. 9, in direct comparison with the fit
493 obtained with the simpler 2-cloud self-consistent retrieval shown earlier in Fig. 1.
494 Similarly, Fig. 10 compares the retrieved cloud profiles (in units of optical depth/bar
495 at 1.6 μm). The slight reduction with height of the optical depth/bar of the hazes
496 (which is constant with height in the SFK2011 model) is due to slight differences in
497 the way we model the aerosols in NEMESIS in terms of their specific density
498 (particles/gram) and fractional scale height. However, these differences are not
499 significant here where we basically have two vertically extended haze layers. We find
500 the SFK2011 model gives a reasonably good fit to the measured spectrum, but that the
501 fit is slightly worse than 2-cloud model ($\Delta\chi^2$= 70, using the number of spectral points
502 n=442), especially in the peaks at λ < 1 μm, where the model predicts too little
503 reflection compared with the T2013 scheme. Figure 8 shows that at these wavelengths

504 we are sensitive to reflection from the LTC as well as the MTC and UTC, which in
505 the SFK2011 scheme has similar scattering properties across the whole range in
506 contrast with the tropospheric cloud of Tice et al. (2013) which is significantly more
507 scattering at short wavelengths than at longer wavelengths. Hence, we replaced the
508 scattering properties of the LTC with particles having scattering properties consistent
509 with those recommended by T2013 for the TC. We assumed a standard Gamma
510 particle-size distribution with mean radius 1.2 μm and variance 0.05 and set the real
511 part of the refractive index to 1.4 at a wavelength of 0.9 μm. We then empirically
512 adjusted the imaginary refractive index spectra, computing the real part with a
513 Kramers-Kronig calculation until we arrived at particles that had the same single-
514 scattering albedo spectra as the T2013 Tropospheric Cloud, but self-consistent cross-
515 section and phase-function spectra. The modified LTC parameters are listed in Table
516 3. Using these updated LTC scattering properties we re-ran our retrieval to derive the
517 revised fit also shown in Fig. 9, which can be seen to fit very well at all wavelengths
518 and fits slightly better than the 2-cloud model ($\Delta\chi^2$= 6.2). In this retrieval we also
519 revised the complex refractive index spectrum of the UTC to be those of methane ice
520 (Martonchik and Orton, 1994), although we found that this change had very little
521 effect on the calculated spectrum as the refractive indices were not greatly different
522 from those assumed by SFK2011 and the fitted opacity of this layer was low. The
523 revised cloud structure of the modified-LTC model is shown in Fig. 10, while the
524 revised complex refractive index spectra of the TH and MTC (assuming an a priorr
525 imaginary refractive index n_i = 0.001) are shown in Fig. 11 (and listed in Table 4).
526 These refractive index spectra can be seen to be almost identical to those derived for
527 the two-cloud T2013 model, shown in Fig. 3. They were also practically identical
528 with the refractive indices retrieved from the unmodified-LTC 5-cloud model (not

shown). We also tested the sensitivity to the *a priori* values of n_i and determined very similar dependencies to the simpler 2-cloud model shown in Figs. 4 and 5.

Thus, by fitting the optical properties of the MTC and TH, and resetting the properties of the LTC we have derived a cloud profile that is consistent with the general structure of the SFK2011 model, but which also provides a spectrum that is consistent with IRTF/SpeX observations over the full range from 0.8 to 1.8 μm. With some refinement of the scattering properties in the 0.3 to 0.8 μm range the fit could easily be extended to the cover the HST/STIS spectral range (0.3 to 1.0 μm) also. However, we do not have access to these data and thus such an extension is beyond the scope of this paper.

As just mentioned, the retrieved imaginary refractive index spectra of the MTC and TH (shown in Fig. 11 and listed in Table 4) are very similar to those previously retrieved with the 2-cloud self-consistent model for the TC and TH (Fig. 3). Again, we find that the lower tropospheric clouds must have increased imaginary index of refraction at wavelengths $\lambda > 1$ μm in order to lower the single scattering albedo and thus suppress of the reflectance of the $\lambda > 1$ μm peaks relative to the $\lambda < 1$ μm peaks. The retrieved particle sizes are also similar with the mean radius of the particles in the Middle Tropospheric Cloud (MTC) being found to be 0.86±0.04 μm, while in the Tropospheric Haze we derive a mean particle size of 0.13±0.02 μm. Again, we found we were insensitive to the variances of these size distributions. Comparing the retrieved errors with the *a priori* errors, we find that only the mean size of the particles in the TH are well constrained. This is better summarised in Table 5, where we compare the *a priori* and retrieved values (together with errors) for all non-imaginary-refractive-index parameters and include an improvement factor, which

indicates how well the value of a parameter has been constrained by the retrieval. Here, it can be seen that the pressure of the MTC has not varied far from that determined by SFK2011 and lies in the region previously retrieved for Uranus' main cloud deck with this methane abundance profile.

The effect of the retrieved refractive index spectra on the actual scattering properties of the MTC and TH can be seen in Figs. 12 and 13, where we have plotted the retrieved extinction cross-section and single-scattering albedo spectra of the Middle Tropospheric Cloud (MTC) and Tropospheric Haze (TH) together with the Henyey-Greenstein scattering parameters that have been fitted to the Mie-calculated phase functions for the a priori $n_i = 0.001$ case. Figures 12 and 13 also show the cloud scattering properties of Tropospheric particles assumed by SFK2011 for reference.

5. Discussion

The retrieved complex refractive index spectra of the particulates should help us in identifying their composition. Unfortunately, the literature contains relatively little information on the complex refractive index spectra of different candidate Uranus condensates in the near-IR range. What data that are available relate to pure, fresh condensates, and not the photochemically altered particles that are likely to exist in Uranus' atmosphere. In Fig. 14 we have compared the retrieved refractive index spectra of our Tropospheric Cloud (TC), using our best-fitting 2-cloud self-consistent model with published data for methane ice (Martonchik and Orton, 1994), ammonia ice (Martonchik, Orton and Appleby, 1984; Howett et al., 2007), solid NH_4SH (Howett et al., 2007) and water droplets (Hale and Querry, 1973). As can be seen, little can be discerned from the variation in wavelength of the derived real component of the refractive index spectrum. For the imaginary part, most candidate condensates

577 have increasing absorption at longer wavelengths, but not to the extent apparently
578 required, suggesting there is an additional unknown source of absorption existing for
579 the Uranus particulates. Possible candidates for the optically thickest scattering cloud
580 at ~2 bars are NH_3, H_2S and perhaps some component of PH_3 ice. However, we can
581 see from Fig. 14 that the scattering properties of pure ammonia ice are clearly
582 inconsistent with those required for Uranus main scattering cloud at the ~2 bar level
583 and the scattering properties of H_2S and PH_3 ice are unknown. Furthermore the high
584 value of the real refractive index for NH4SH would suggest that this particle is not
585 suitable either since we saw earlier that our method indicates that particles with real
586 refractive index in the range 1.2-1.4 provide the best fit to the observed spectrum. Of
587 course, there is no certainty that the particles in the main cloud deck are pure
588 condensates at all. Photochemically produced haze particles may settle down from the
589 stratosphere and upper troposphere and coat the fresh condensates, in a process akin
590 to riming, and in the process mask their pure scattering properties. Using an
591 Equilibrium Cloud Condensation Model, and assuming generally accepted deep
592 enrichment factors of O/H = 100 × Solar, N/H = Solar, S/H = 11 × Solar and C/H =
593 40 × Solar (Irwin, 2009) it is found that NH_4SH should condense at a pressure of ~13
594 bars, well below the observable level, leaving an H_2S cloud to condense at ~5 bars. Of
595 course, if the N/S ratio is closer to unity it might be that more of the H_2S is combined
596 with NH_3 in a deep NH_4SH cloud, leaving a small remnant of H_2S to condense at the
597 lower pressures determined here. It should also be noted that if N/S > 1, then all the
598 H_2S will be combined in a lower NH_4SH cloud, leaving NH_3 free to condense at
599 lower pressures, although we have seen that in its pure form NH_3 ice particles are too
600 reflective at all wavelengths to be consistent with the required scattering properties.
601 This view is also inconsistent with ground-based microwave observations (de Pater

602 and Massie, 1985), which finds that the abundances of both water and ammonia are
603 substantially sub-solar (by factors of ~100) down to pressures of ~50 bars, but that
604 H_2S is much more abundant (10 – 35 × solar). To solve the identification of Uranus'
605 main cloud clearly requires laboratory measurements of the complex refractive index
606 spectrum of H_2S and PH_3, although if the particles are heavily coated with
607 photochemical products drizzling down from above, they are likely not pure anyway
608 and determining their bulk composition spectroscopically may not be possible.

609 The latitudinal distribution of methane in Uranus' upper troposphere was found
610 by Karkoschka and Tomasko (2009) to vary significantly with latitude, from
611 abundances of ~4% at equatorial latitudes to < 2% near the poles. This distribution
612 has since been confirmed by Sromovsky et al. (2011), Irwin et al. (2012b) and Tice et
613 al. (2013). The distribution bears a remarkable similarity with ground-based
614 microwave obsrvations of Uranus with the VLA (de Pater et al. 1991; Hofstadter and
615 Butler 2003) which find that the deep abundance of NH_3 at pressures < 50 bars
616 decreases by almost an order of magnitude from equatorial latitudes towards the
617 poles. Such a variation is consistent with a large Hadley Cell in Uranus' atmosphere
618 with air rising at the equator and descending at the poles, or with an atmosphere that
619 is convectively overturning at low latitudes, but becomes convectively suppressed at
620 latitudes polewards of 45° N,S. The fact that methane has such a similar latitudinal
621 variation suggests that the abundances of ammonia and methane are likely linked.
622 Such a view seems inconsistent with the circulation pattern suggested by SFK2011
623 (their Fig. 18), which shows a similar looking Hadley cell at pressures less than 3
624 bars, but which reverses at deeper pressures.

625 Finally, we noted earlier that our approach of modelling the scattering
626 characteristics of ice particles with Mie scattering, which assumes spherical particles

may represent a cause of systematic error, since the phase functions of spherical particles contain features, such as the 'rainbow' and 'glory', that are absent from the phase functions of a distribution of randomly orientated non-spherical particles. We have partly ameliorated this potential drawback by approximating the Mie-scattering phase functions with best-fitting combined Henyey-Greenstein phase functions, but systematic errors remain possible. We are currently in the process of updating our model to use pre-tabulated scattering properties calculated for a range of non-spherical particles by Dobovik et al. (2006), which should correct for such potential errors (although adding another degree of freedom to the model – the particle shape). However, this development is still in progress and hence beyond the scope of this paper.

6. Conclusions

The retrieval mechanism developed here represents a significant improvement over previous modelling studies of near-IR Uranus spectra. By retrieving the imaginary refractive index spectra of the clouds and constructing the real part of the refractive index through a Kramers-Kronig analysis, we are able to determine self-consistent extinction cross-section, single-scattering and phase-function spectra for the clouds and hazes in Uranus' atmosphere over the range 0.8 to 1.8 μm. We find that we require particles in the main cloud deck at ~2 bars to be significantly more absorbing at wavelengths $\lambda > 1.0$ μm than they are at shorter wavelengths $\lambda < 1.0$ μm, which provides a potential constraint on the identity of the main particle type. We find that the scattering properties required are inconsistent with pure ammonia ice and we thus recommend that laboratory studies be conducted to establish if H_2S or PH_3, which might also potentially condense at these pressures, have such scattering properties

651 which would then potentially identify them as being the main cloud condensate in
652 Uranus' atmosphere.

653 In addition to developing the new retrieval scheme we compared the 2-cloud-
654 layer model of Tice et al. (2013), using the methane profile of Baines et al. (1995)
655 with the 5-cloud-layer model of Sromovsky, Fry and Tomasko (2011), using their
656 reanalysed 'F1' Voyager 2 radio-occultation profile. We note here that we also fitted
657 the spectra with the 2-cloud scheme using the 'F1' profile and found a reasonable fit,
658 but poorer than that obtained when using the Baines et al. (1995) profile and worse
659 also than when using the Spitzer profile (Orton et al. 2014). We find that both 2-cloud
660 and 5-cloud models reproduce well the observed centre-of-disc IRTF/Spex spectrum
661 of Uranus, recorded in 2009. However, it can be seen in Fig. 9 that a modified version
662 of the SFK2011 model does fit the observations significantly better at shorter
663 wavelengths and the 'F1' profile has the added advantage of being based on a
664 temperature/abundance profile that is simultaneously consistent with the enhanced
665 equatorial abundaces of methane determined by Karkoschka and Tomasko (2009) and
666 leads to methane condensation at 1.2 bars, where the Voyager 2 radio-occultation
667 profile noted a distinct step in the refractivity gradient. We should note, however, that
668 the 'F1' profile of SFK2011 requires a He/H_2 ratio that lowers the tropopause
669 temperatures, and indeed the entire temperature profile above the CH_4 condensation
670 level, to values too cold to be consistent with Spitzer IRS observations. We find that
671 we retrieve similar refractive index spectra for the main cloud at ~2 bars using both
672 approaches. However, this analysis does not lead to a very clear indication of which
673 profile is most consistent with the IRTF/SpeX observations, although the 5-cloud
674 model does seem to improve slightly the fit at wavelengths less than 1 μm.

675 **Acknowledgements**

676 We are grateful to the United Kingdom Science and Technology Facilities Council for

677 funding this research. Leigh Fletcher was supported by a Royal Society Research

678 Fellowship at the University of Oxford.

679 **Tables**

680

	Tropospheric Cloud				Tropospheric Haze			
λ	n_r	n_i	χ	ϖ	n_r	n_i	χ	ϖ
0.7	1.40014	0.00101	0.99498	0.98547	1.39989	0.00100	13.35856	0.99096
0.8	1.39874	0.00096	1.14211	0.98950	1.39990	0.00099	9.25143	0.98939
0.9	1.39702	0.00068	1.26472	0.99405	1.39990	0.00099	6.59613	0.98760
1.0	1.39448	0.00080	1.33341	0.99411	1.39993	0.00103	4.82549	0.98481
1.1	1.38987	0.00102	1.34484	0.99338	1.39996	0.00102	3.59473	0.98224
1.2	1.38033	0.00418	1.28960	0.97522	1.39997	0.00101	2.71645	0.97939
1.3	1.38607	0.05149	1.13529	0.77422	1.39998	0.00101	2.07951	0.97570
1.4	1.40000	0.01206	1.20073	0.93726	1.40000	0.00099	1.61016	0.97211
1.5	1.38728	0.03687	1.05920	0.83024	1.40000	0.00097	1.26102	0.96826
1.6	1.39696	0.06189	1.00000	0.74939	1.39999	0.00098	1.00000	0.96281
1.7	1.43592	0.00467	1.11423	0.97672	1.39997	0.00102	0.80312	0.95540
1.8	1.42657	0.00118	1.01875	0.99390	1.39998	0.00103	0.65161	0.94815
1.9	1.42104	0.00100	0.93042	0.99472	1.40002	0.00101	0.53326	0.94201

681 Table 1. Derived scattering properties of the Tropospheric Cloud and Tropospheric
682 Haze using 2-cloud Tice et al. (2013) model, with the *a priori* imaginary refarctive
683 index, n_i, set to 0.001±50% at all wavelengths. The imaginary part of the refractive
684 index spectrum (n_i) is retrieved by the model and a Kramers-Kronig analysis used to
685 construct the real part (n_r). The complex refractive index spectrum is then used in a
686 Mie-scattering calculation to constuct the extinction efficiency (χ, normalised to 1.6
687 μm) and single-scattering albedo (ϖ) spectra. The errors on these fitted and derived
688 quantities is best understood by inspection of Figures 5 and 6, which show the
689 retrieved quantities obtained for different *a priori* values of n_i.

Cloud	p_{Base} (bar)	p_{Top} (bar)	Cross section	Single scattering albedo	Phase function
Stratospheric Haze	0.1	0.01 bar	n_r=1.4, $n_i(\lambda)$ = 0.0055exp[(350-λ)/100] (λ in nm), extrapolated from 1-2 μm. Scattering properties computed with Mie scattering, assuming standard Gamma distribution of sizes with r_0 = 0.1 μm and variance=0.3.		
Tropospheric Haze	0.9	0.1	Constant	ϖ(λ)=1−1/[2+exp[(λ-290)/37]] (λ in nm), extrapolated from 1-2 μm.	Henyey Greenstein: g1=0.7, g2=-0.3, f(λ)=0.94-0.47sin4[(1000-l)/445] (λ in nm). f(λ) fixed to f(1.0) at all wavelengths from 1-2 μm.
Upper Tropospheric Cloud (UTC)	1.23	1.14 (1.28 × 0.93)	N=1.4+0i at all wavelengths. Scattering properties computed with Mie scattering, assuming standard Gamma distribution of sizes with r_0 = 1.2 μm and variance=0.1		
Middle Tropospheric Cloud (MTC)	1.68	1.56 (1.68 × 0.93)	As Tropospheric Haze		
Lower Tropospheric Cloud (LTC)	5	4.9 (5 × 0.98)	As Tropospheric Haze		

690 Table 2. Five-cloud layering scheme of Sromovsky, Fry and Karkoschka (2011) and
691 associated cloud scattering properties.

692

λ	n_r	n_i	χ	ϖ
0.7	1.36675	0.00001	0.88527	0.99978
0.8	1.38547	0.00001	0.91996	0.99981
0.9	1.39103	0.00001	1.00000	0.99984
1	1.39029	0.00001	1.11674	0.99987
1.1	1.39802	0.01875	1.17604	0.84218
1.2	1.39552	0.0375	1.20952	0.76656
1.3	1.38551	0.05625	1.20510	0.72023
1.4	1.38071	0.075	1.17185	0.68199
1.5	1.37764	0.075	1.16517	0.69163
1.6	1.37547	0.075	1.14720	0.69793
1.7	1.37385	0.075	1.12095	0.70173
1.8	1.37258	0.075	1.08888	0.70362
1.9	1.37157	0.075	1.05294	0.70403

693 Table 3. Empically determined scattering properties of Lower Tropospheric Cloud
694 (LTC) of the SFK2011 scheme adjusted to match the single-scattering albedo
695 spectrum of tropospheric scatterers determined by Tice et al. (2013). A standard
696 gamma size distribution was assumed with mean radius 1.2 μm and variance 0.05.
697 Again, the extinction efficiency (here normalised to 0.9 μm) and single-scattering
698 albedo spectra were determined from the complex refractive index spectrum using
699 Mie theory.

700

	Middle Tropospheric Cloud				Tropospheric Haze			
λ	n_r	n_i	χ	ϖ	n_r	n_i	χ	ϖ
0.7	1.39713	0.00099	1.08248	0.98682	1.39990	0.00100	17.31323	0.98629
0.8	1.39606	0.00097	1.24206	0.99024	1.39991	0.00099	11.51517	0.98306
0.9	1.39478	0.00089	1.35722	0.99276	1.39991	0.00098	7.87520	0.97908
1.0	1.39261	0.00075	1.40963	0.99476	1.39993	0.00101	5.51755	0.97327
1.1	1.38851	0.00097	1.40061	0.99391	1.39995	0.00102	3.95039	0.96676
1.2	1.38180	0.00628	1.32371	0.96418	1.39997	0.00101	2.88757	0.95978
1.3	1.38813	0.04229	1.18941	0.80838	1.39998	0.00101	2.15559	0.95117
1.4	1.40000	0.00764	1.23239	0.95983	1.40000	0.00100	1.63888	0.94242
1.5	1.38767	0.02202	1.09363	0.89127	1.40000	0.00098	1.26803	0.93294
1.6	1.38985	0.05468	1.00000	0.76820	1.39999	0.00100	1.00000	0.91996
1.7	1.42617	0.00405	1.08911	0.97949	1.39999	0.00102	0.80171	0.90488
1.8	1.41844	0.00112	0.98855	0.99411	1.40000	0.00103	0.65106	0.88990
1.9	1.41397	0.00100	0.89883	0.99459	1.40003	0.00101	0.53427	0.87613

Table 4. Derived scattering properties of Middle Tropospheric Cloud (MTC) and Tropospheric Haze (TH) using the modified SFK2011 model with modifed Lower Tropospheric Cloud (LTC) properties, with the *a priori* imaginary refarctive index, n_i, set to 0.001±50% at all wavelengths. The imaginary part of the refractive index spectrum (n_i) is retrieved by the model and a Kramers-Kronig analysis used to construct the real part (n_r). The errors on these fitted and derived quantities is best understood by inspection of Figures 5 and 6, which show the retrieved quantities obtained for different *a priori* values of n_i.

711

Variable	x_a	e_a	e_a/x_a	x_n	e_n	e_n/x_n	Improve(%)
P_{LTC} (bar)	5.0	fixed	-	5	fixed	-	-
τ_{LTC}	3.45	3.45	1.00	7.20	0.997	0.139	86.1
P_{MTC} (bar)	1.68	0.05	0.0298	1.78	0.025	0.014	53.1
τ_{MTC}	1.28	1.28	1.00	1.49	0.077	0.0521	94.8
P_{UTC} (bar)	1.23	fixed	-	1.23	fixed	-	-
τ_{UTC}	0.322	0.322	1.00	0.087	0.0195	0.224	77.6
τ_{TH}	0.01	0.01	1.00	0.0019	0.000129	0.068	93.2
τ_{SH}	0.0012	0.0012	1.00	0.0003	0.000083	0.274	72.6
r_{MTC}	1.00	0.05	0.05	0.86	0.037	0.0433	13.3
b_{MTC}	0.05	0.01	0.2	0.0495	0.0099	0.1994	0.3
r_{TH}	0.1	0.05	0.5	0.1309	0.0205	0.1565	68.7
b_{TH}	0.05	0.01	0.2	0.0507	0.0101	0.1994	0.3

712 Table 5. Retrieved non-imaginary-refractive-index parameters for the 5-cloud
713 SFK2011 model with modified LTC applied to the IRTF/SpeX centre-of-disc Uranus
714 spectra. Here x_a, e_a are the *a priori* values and errors, x_n, e_n are the retrieved values
715 and errors. These parameters are held as log(values) by NEMESIS and hence the
716 improvement factor is defined as $100\times\left(1-(e_n/x_n)/(e_a/x_a)\right)$ and indicates how far
717 the retrieved error limits differ from the *a priori*. Values with a high improvement
718 factor are well constrained by the retrieval.

719

720 **References**

721 Baines, K.H., Mickelson, M.E., Larson, L.E. Ferguson, D.W. 1995. The abundances
722 of Methane and ortho/para Hydrogen on Uranus and Neptune: Implications of new
723 laboratory 4-0 H_2 quadrupole line parameters. Icarus 114, 328 – 340.

724 Borysow, A. 1991. Modeling of collision-induced infrared absorption spectra of H_2-
725 H_2 pairs in the fundamental band at temperatures from 20 to 300 K. Icarus 92,
726 273 – 279 .

727 Borysow, A. 1992. New model of collision-induced infrared absorption spectra of H_2-
728 He pairs in the 2-2.5 micron range at temperatures from 20 to 300 K - an update.
729 Icarus 96, 169 – 175.

730 Borysow, A., Borysow, J., Fu, Y. 2000. Semi-empirical model of collision-induced
731 absorption spectra of $H_2 – H_2$ complexes in the second overtone band of hydrogen
732 at temperatures from 50 to 500K. Icarus 145, 601 – 608.

733 de Pater, I., Massie, S. 1985. Models of the millimeter-centimeter spectra of the giant
734 planets. Icarus 62, 143 – 171.

735 de Pater, I., Romani P.N., Atreya, S.K. 1991. Possible microwave absorption by H_2S
736 gas in Uranus' and Neptune's atmospheres. Icarus 91, 220 – 233.

737 Dubovik, O., Sinyuk, A., Lapyonok, T., Holben, B.N., Mishchenko, M., Yang, P.,
738 Eck, T.F., Volten, H., Munoz, O., Veihelmann, B., van der Zande, W.J., Leon, J.-
739 F., Sorokin, M., Slutsker, I. 2006. Application of spheroid models to account for
740 aerosol particle nonsphericity in remote sensing of desert dust. J. Geophys. Res.
741 111, D11209, doi:10.1029/2005JD006619

742 Goody, R.M., West, R., Chen, L., Crisp, D. 1989. The correlated-k method for
743 radiation calculations in nonhomogeneous atmospheres. J.Q.S.R.T. 42, 539 – 550.

744 Goody, R.M., Yung, Y.L. (1989) Atmospheric Radiation: Theoretical Basis (Second
745 Edition). Oxford University Press, Oxford. UK.

746 Hansen, J.E., Travis, L.D. 1974. Light scattering in planetary atmospheres. Space Sci.
747 Rev. 16, 527 – 610.

748 Hale, G.M., Querry, M.R. 1973. Optical Constants of Water in the 200-nm to 200-μm
749 Wavelength Region, Appl. Opt. 12, 555 – 563.

750 Hofstadter, M.D., Butler, B.J. 2003. Seasonal change in the deep atmosphere of
751 Uranus. Icarus 165, 168 – 180.

752 Howett, C.J.A., Carlson, R.W., Irwin, P.G.J., Calcutt, S.B. (2007) Optical constants of
753 ammonium hydrosulfide ice and ammonia ice. J. Opt. Soc. Am., B, 24, 126 – 136.

754 Irwin, P.G.J., Teanby, N.A., Davis, G. R. 2007. Latitudinal Variations in Uranus'
755 Vertical Cloud Structure from UKIRT UIST Observations, Ap. J., 665, L71-L74.

756 Irwin, P.G.J., Teanby, N.A., de Kok, R., Fletcher, L.N., Howett, C.J.A., Tsang,
757 C.C.C., Wilson, C.F., Calcutt, S.B., Nixon, C.A., Parrish, P.D. 2008. The
758 NEMESIS planetary atmosphere radiative transfer and retrieval tool. J. Quant.
759 Spectrosc. and Rad. Trans. 109, 1136 – 1150.

760 Irwin, P.G.J., Teanby, N.A., Davis, G. R. 2009. Vertical cloud structure of Uranus
761 from UKIRT/UIST observations and changes seen during Uranus' Northern Spring
762 Equinox from 2006 to 2008. Icarus 203, 287 – 302

763 Irwin, P.G.J, Teanby, N.A., Davis, G.R. 2010. Revised vertical cloud structure of
764 Uranus from UKIRT/UIST observations and changes seen during Uranus'
765 Northern Spring Equinox from 2006 to 2008: Application of new methane
766 absorption data and comparison with Neptune. Icarus 208, 913 – 926.

767 Irwin, P.G.J., Teanby, N.A., Davis, G.R., Fletcher, L.N., Orton, G.S., Tice, D.,
768 Kyffin, A. 2011. Uranus' Cloud Structure and Seasonal Variability from Gemini-
769 North and UKIRT observations. Icarus 212, 339 – 350.

770 Irwin, P.G.J., Teanby, N.A., Davis, G.R., Fletcher, L.N., Orton, G.S., Calcutt, S.B.,
771 Tice, D.S., Hurley, J. 2012a. Further seasonal changes in Uranus' Cloud Structure
772 observed by Gemini-North and UKIRT. Icarus 218, 47 – 55.

773 Irwin, P.G.J., de Bergh, C., Courtin, R., Bézard, B., Teanby, N.A., Davis, G.R.,
774 Fletcher, L.N., Orton, G.S., Calcutt, S.B., Tice, D., Hurley, J. 2012b. The
775 application of new methane line absorption data to Gemini-N/NIFS and
776 KPNO/FTS observations of Uranus' near-infrared spectrum. Icarus 220, 369 – 382.

777 Irwin, P.G.J. 2009. Giant planets of our solar system: Atmospheres, composition and
778 structure. Springer-Praxis Publishing.

779 Karkoschka, E., Tomasko, M. 2009. The haze and methane distributions on Uranus
780 from HST-STIS spectroscopy. Icarus 202, 287 – 302

781 Karkoschka, E., Tomasko, M. 2010. Methane absorption coefficients for the jovian
782 planets from laboratory, Huygens, and HST data. Icarus 205, 674 – 694.

783 Lacis, A.A., Oinas, V. 1991. A description of the correlated-k distribution method for
784 modelling nongray gaseous absorption, thermal emission, and multiple scattering
785 in vertically inhomogenous atmospheres. J. Geophys. Res. 96, 9027 – 9063.

786 Martonchik, J.V., Orton, G.S., Appleby, J.F. 1984. Optical properties of NH3 ice
787 from the fra infrared to the near ultraviolet. Appl. Opt., 23, 541 – 547.

788 Martonchik, J.V., Orton, G.S. 1994. Optical constants of liquid and solid methane.
789 Appl. Opt. 33, 8306 – 8317.

790 Orton, G.S., Fletcher, L.N., Moses, J.I., Mainzer, A.K., Hines, D., Hammel, H.B.,
791 Martin-Torres, F.J., Burgdorf, M., Merlet. C., Line, M.R. 2014. Mid-Infrared
792 Spectroscopy of Uranus from the Spitzer Infrared Spectrometer: 1. Determination
793 of the Mean Temperature Structure of the Upper Troposphere and Stratosphere.
794 Icarus (in press).
795 Sheik-Bahae, M. 2005. "Nonlinear Optics Basics. Kramers–Kronig Relations in
796 Nonlinear Optics". In Robert D. Guenther. *Encyclopedia of Modern Optics*.
797 Amsterdam: Academic Press.
798 Sromovsky, L. A., Irwin, P.G.J., Fry, P.M. 2006. Near-IR methane absorption in outer
799 planet atmospheres: Improved models of temperature dependence and implications
800 for Uranus cloud structure, Icarus 182, 577-593.
801 Sromovsky, L.A., Fry, P.M., Kim, J.H. 2011. Methane on Uranus: The case for a
802 compact CH_4 cloud layer at low latitudes and a severe CH_4 depletion at high
803 latitudes based on a re-analysis of Voyager occultation measurements and STIS
804 spectroscopy. Icarus 215, 292 – 312.
805 Tice, D.S., Irwin, P.G.J., Fletcher, L.N., Teanby, N.A., Hurley, J., Orton, G.S., Davis,
806 G.R. 2013. Uranus' cloud particle properties and latitudinal methane variation
807 from IRTF SpeX observations. Icarus 223, 684 – 698.
808 Zheng, C., Borysow, A. 1995. Modeling of collision-induced infrared absorption
809 spectra of H_2 pairs in the first overtone band at temperatures from 20 to 500 K.
810 Icarus 113, 84 – 90.
811

812 **Figures**

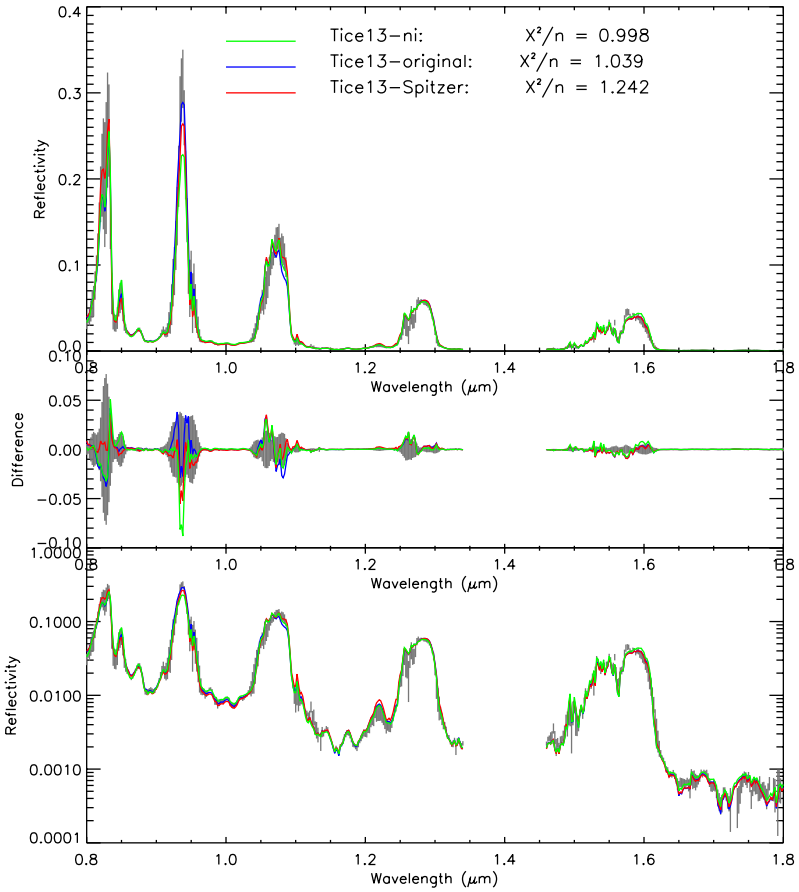

813

814 Figure 1. Measured IRTF/SpeX spectrum at 1.3ºS (thick grey line indicates
815 mesurement and random error) and fit to it with the 2-cloud model of T2013 using
816 three different methods: 1) self-consistent scattering property retrieval (green), 2)
817 original T2013 model with empirically determined scattering properties (blue) and 3)
818 original T2013 model with empirically determined scattering properties, but using the
819 Sptizer temperature-abundance profile (red). The top panel shows the reflectivity
820 spectrum (I/F) in linear space, with the differences shown in the middle panel. The
821 bottom panel shows the reflectivity space in log space to accentuate the strong
822 methane-absorbing regions. The χ^2/n of the fits are shown in the top panel. The

spectrum between 1.34 and 1.46 μm is not accurately measured by IRTF due to telluric water absorption and so has been omitted here.

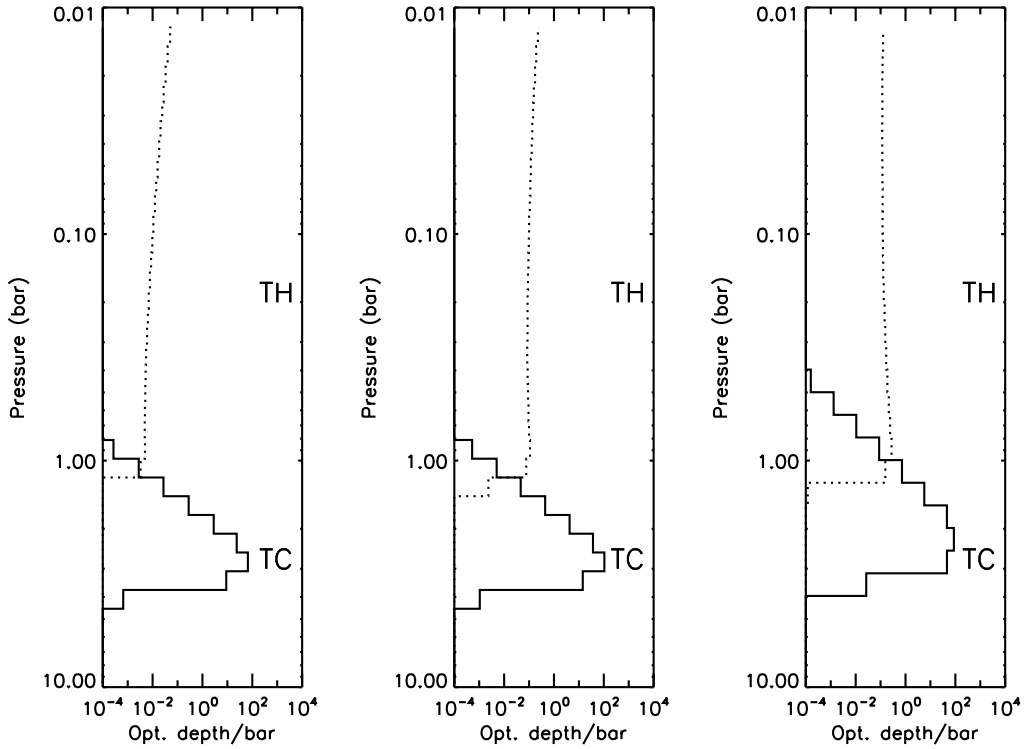

Figure 2. Fitted cloud density profiles (in units of optical depth/bar at 1.6 μm) for the 2-cloud T2013 model using: 1) self-consistent scattering particles retrieval and T2013 atmospheric model (left panel), 2) T2013's empirically adjusted scattering parameters and the T2013 atmospheric model (middle panel), and 3) T2013's empirically adjusted scattering parameters and the Spitzer atmospheric model (right panel). As can be seen very similar cloud structres are inferred with the self-consistent retrieval approach and the original T2013 method. For the Spitzer temperature-abundance profile, which has a higher deep methane abundance, the TC moves to slightly lower pressures as expected.

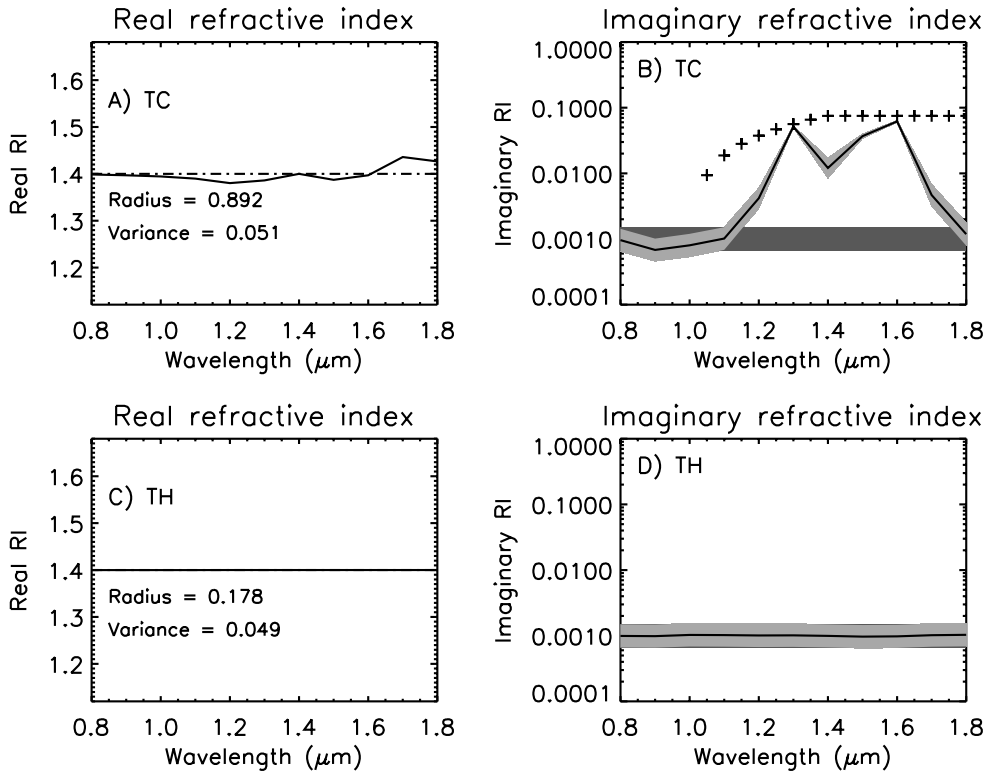

835

836 Figure 3. Fitted complex refractive indices of the Tropospheric Cloud (TC) and
837 Tropospheric Haze (TH) using the 2-cloud model with our self-consistent scattering
838 parameter retrieval, with *a priori* imaginary refractive index for both particle types set
839 to 0.0010±0.0005 (i.e. 50%). The *a priori* imaginary refractive index spectrum and
840 errors are shown as the dark grey region, while the fitted spectrum and errors are
841 shown as the light grey region and superposed solid lines. The *a priori* real refractive
842 index spectra are shown by the dot-dash lines and the inferred Kramers-Kronig
843 spectrum by the solid line. The cross symbols show the imaginary refractive indices
844 necessary to reproduce the single-scattering albedo spectra inferred for the TC by
845 Tice et al. (2013). Comparing the size of the error bars we can see that the imaginary
846 refractive index of the TC particles is well constrained in the absorption peaks at 1.3
847 ands 1.6 μm, but is less well contrained elsewhere. The imaginary refractive index of
848 the TH particles is not well constrained using this single observed spectrum.

849

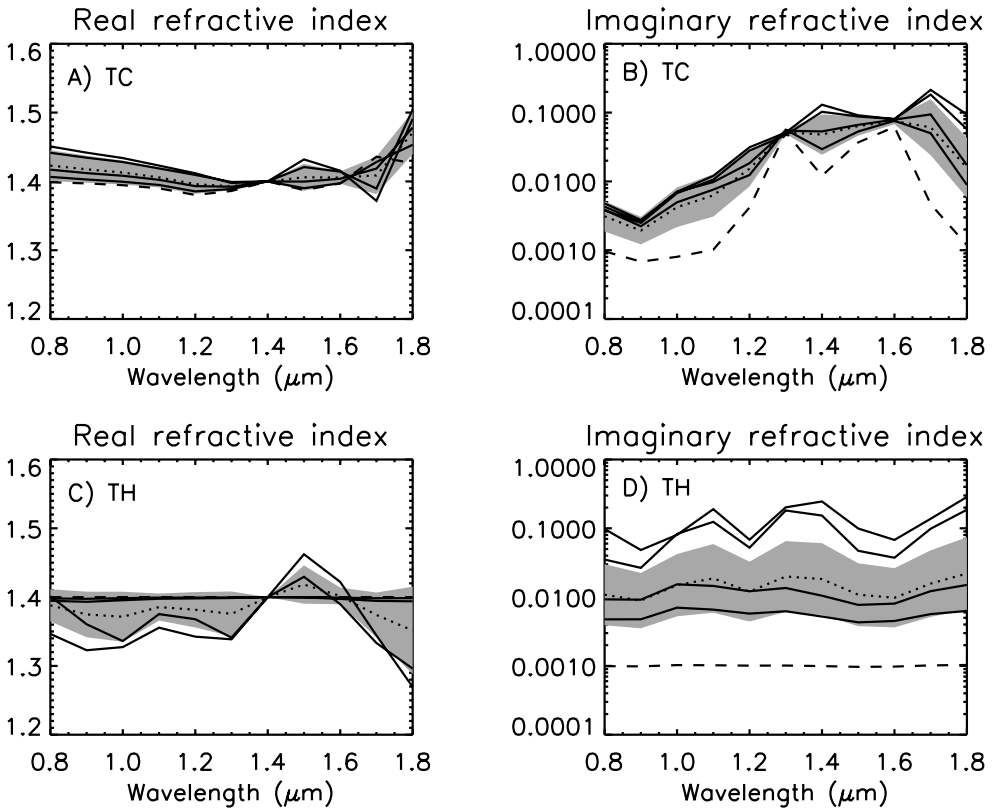

850

851 Figure 4. Fitted complex refractive indices of the Tropospheric Cloud (TC) and
852 Tropospheric Haze (TH) using the 2-cloud model with self-consistent scattering
853 parameter retrieval, with *a priori* imaginary refractive index for both particle types set
854 to 0.001, 0.005, 0.01, 0.05 and 0.1 (all ±50%). The solid lines are the individual cases,
855 except the case where n_i=0.001 for which a dashed line is used. The mean of all five
856 cases are the dotted lines with standard deviation indicated by the grey region. The
857 same variation of imaginary refractive index with wavelength is found in all five
858 cases for the TC particles, but there is much less constraint on the TH particles.

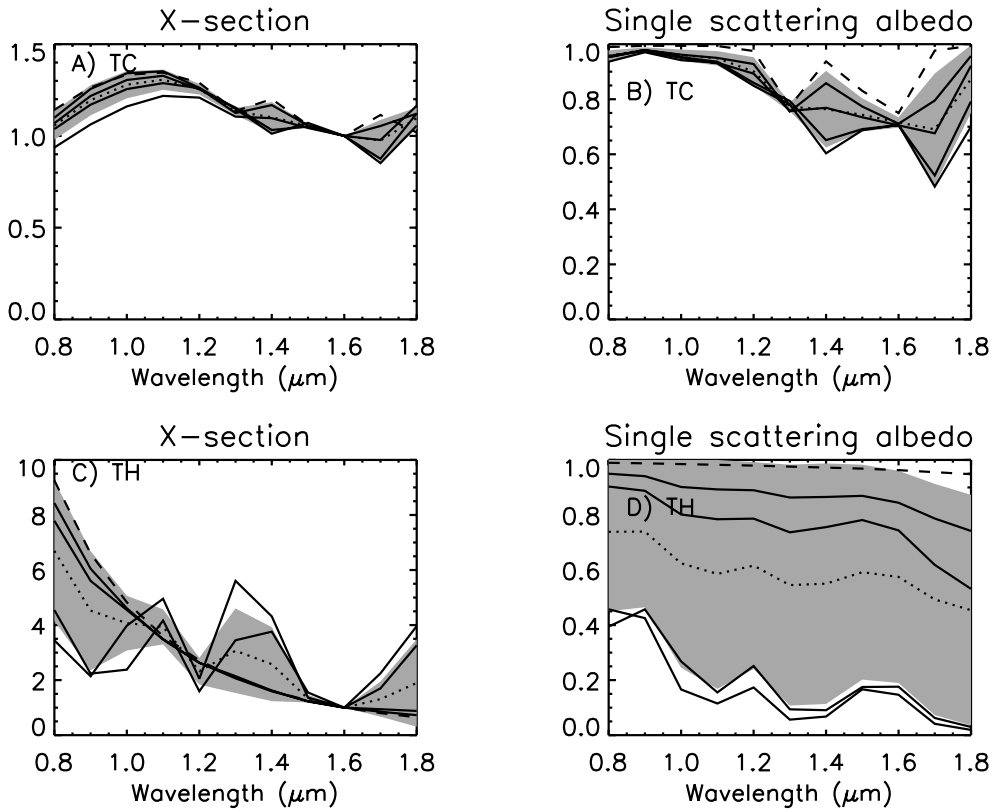

859

860 Figure 5. Fitted cross-section (normalised at 1.6 μm) and single scattering albedoes
861 of the Tropospheric Cloud (TC) and Tropospheric Haze (TH) using the 2-cloud model
862 with self-consistent scattering parameter retrieval, with *a priori* imaginary refractive
863 index for both particle types set to 0.001, 0.005, 0.01, 0.05 and 0.1 (all ±50%). The
864 line styles are identical to those used in Fig. 4. As can be seen the proporties of the
865 TC particles are well constrained, but there is considerable degeneracy in the
866 solutions for the TH particles.

867

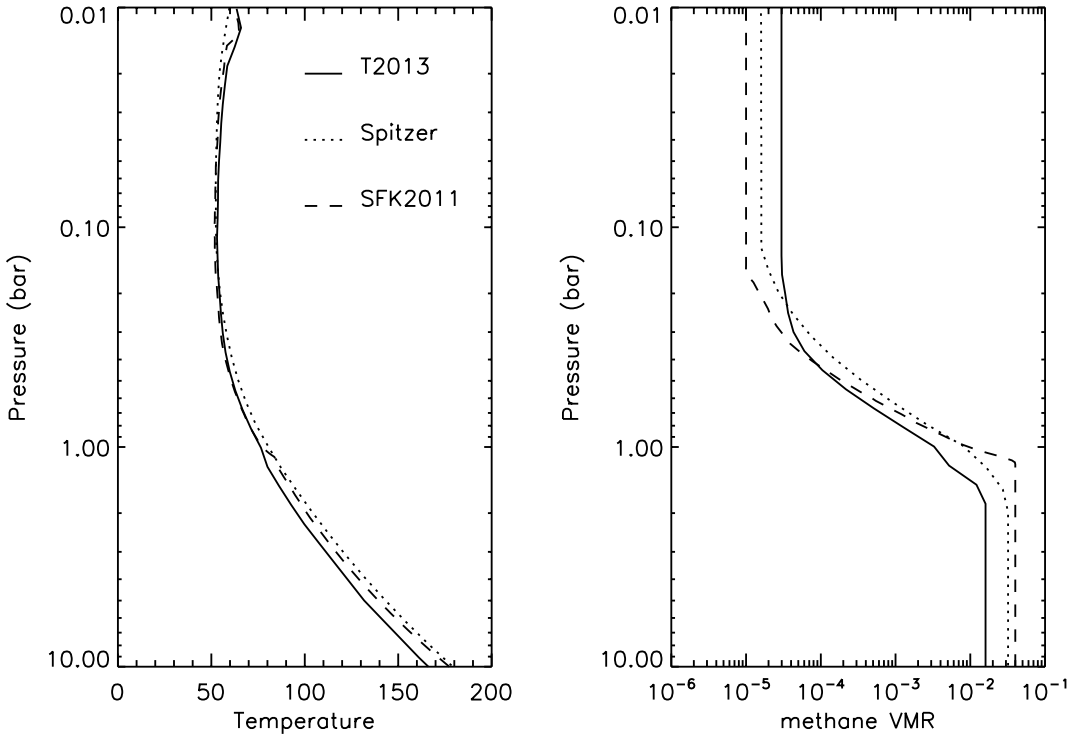

868

869 Figure 6. Comparison of the different vertical profiles of temperature and methane
870 assumed in this study, namely the Baines et al. (1995) profile used by T2013, the
871 Spitzer profile (Orton et al., 2014), and the 'F1' profile of SFK2011.

872

873

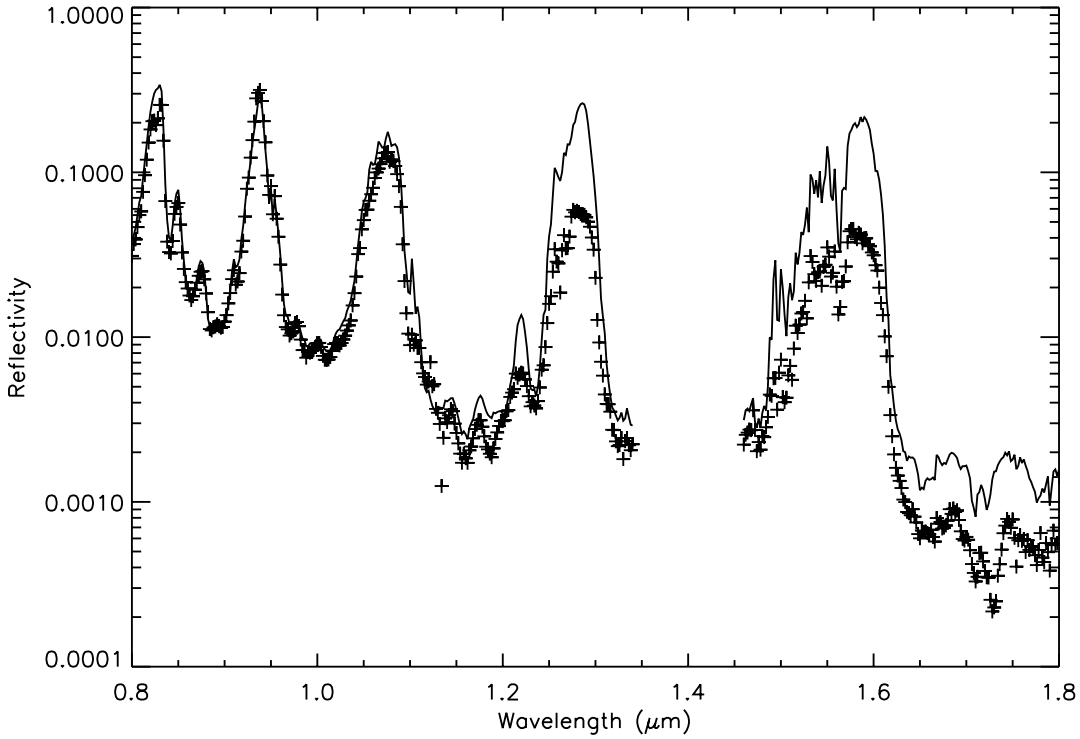

874

875 Figure 7. Measured Uranus spectrum observed by IRTF/SpeX at 1.3°S (cross
876 symbols) together with synthetic spectrum calculated with the published SFK2011
877 cloud model, without any modification. The synthetic spectrum at wavelengths less
878 than 1 μm, which the model was designed to fit, shows a good correspondence with
879 the IRTF/SpeX spectrum (although the reflectance in the 0.8 and 1.15 μm peaks is a
880 little low), but the agreement becomes increasingly poor at longer wavelengths.

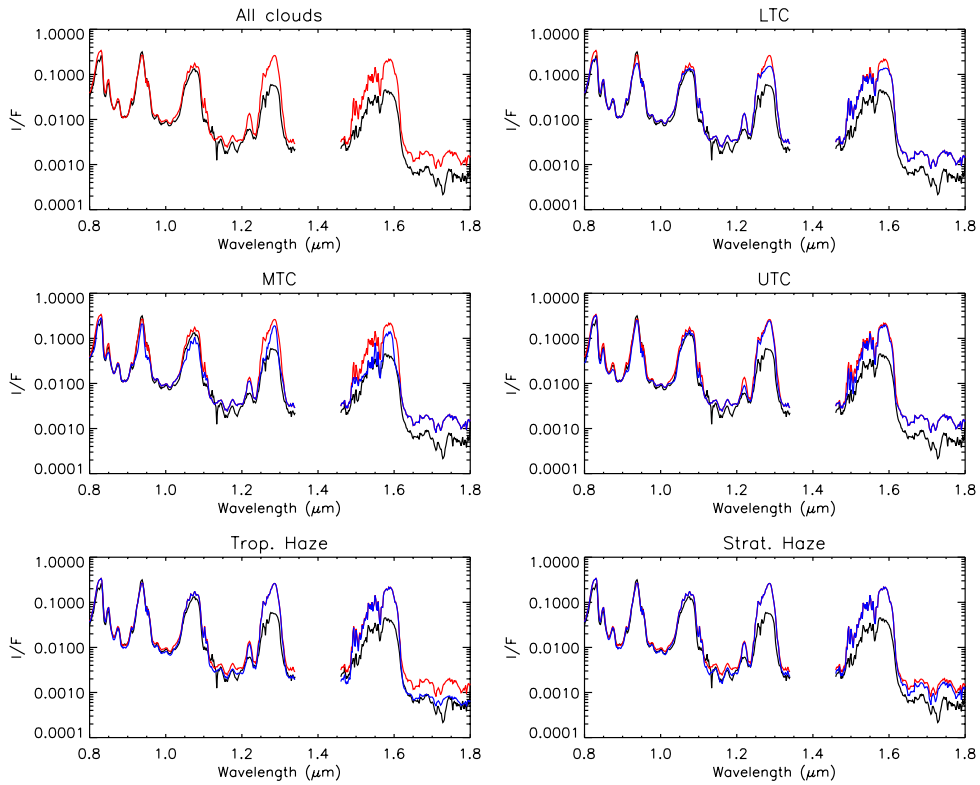

881

882 Figure 8. Effect of removing in turn the contribution to the synthetic spectrum of each
883 cloud layer of the SFK2011 cloud model. In each plot the measured IRTF/SpeX
884 spectrum at 1.3°S is indicated by the black line and the spectrum calculated from the
885 standard SFK2011 model is shown in red. The spectrum calculated with one of the
886 cloud layers removed is shown by the blue lines in the separate panels.

887

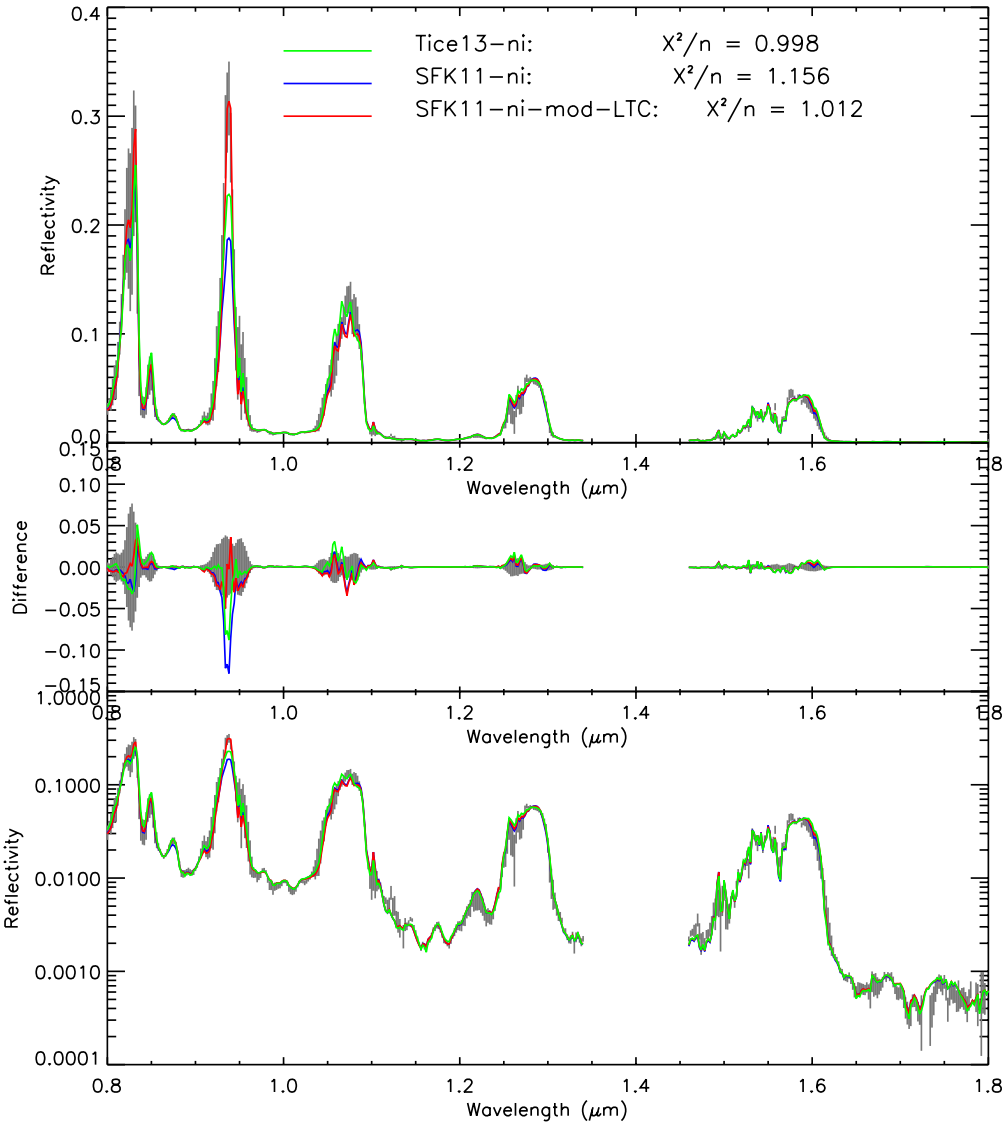

888

889 Figure 9. Measured IRTF/SpeX spectrum at 1.3ºS (thick grey line indicates
890 mesurement and random error) and fit to it with with self-consistent retrieval model
891 using 1) a 2-cloud model of T2013 (green), 2) the first modification of the cloud
892 model of SFK2011 (blue), and the final modification of this model (red) with
893 modified LTC properties. Again the top panel shows the reflectivity spectrum (I/F) in
894 linear space with the differences shown in the middle panel. The bottom panel shows
895 the reflectivity space in log space. The χ^2/n of the fits are shown in the top panel. The

spectrum between 1.34 and 1.46 μm is not accurately measured by IRTF due to telluric water absorption and so has been omitted here.

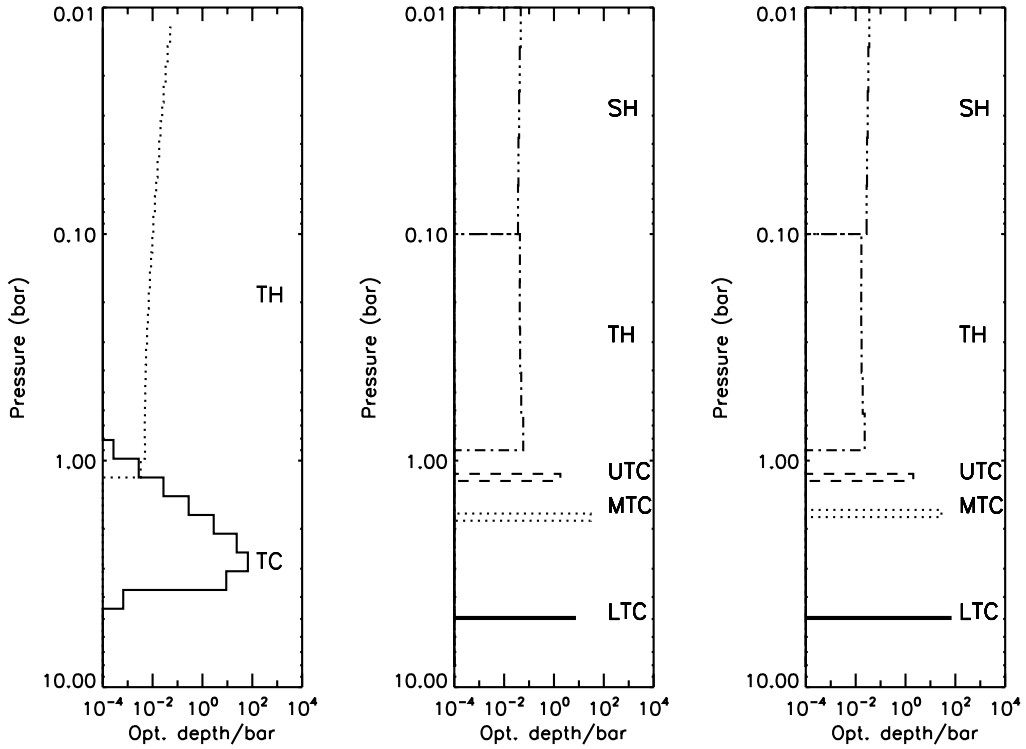

Figure 10. Fitted cloud density profiles (in units of optical depth/bar at 1.6 μm) for the: 1) 2-cloud self-consistent model (left panel), 2) the modified SKF2011 model using their LTC properties (middle), and the modified SKF2011 model using revised LTC properties consistent with the TC of T2013 (right panel). Opacities are here referred to their values at 1.6 μm, not to the normalising wavelength of 0.9 μm used by SFK2011.

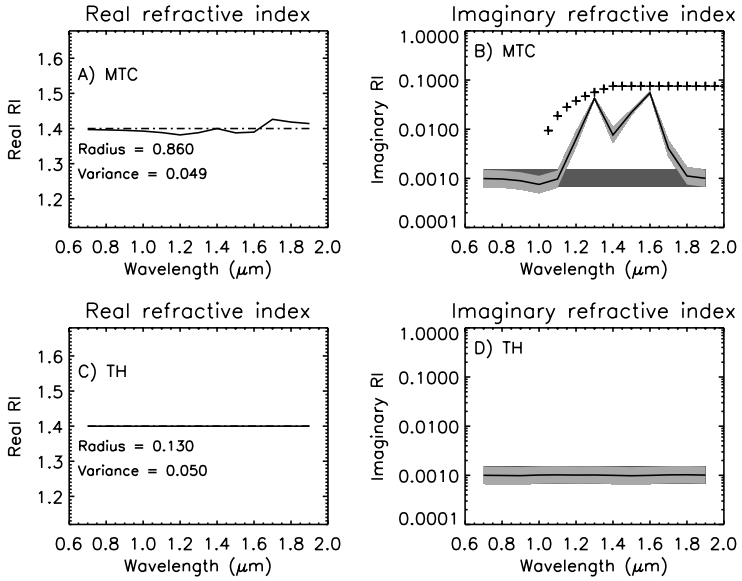

906

907 Figure 11. Fitted spectral properties of the Middle Tropospheric Cloud (MTC) and
908 Tropospheric Haze (TH) using the modified SFK2011 5-cloud model, with revised
909 spectral properties of the Lower Tropospheric Cloud (LTC). The linestyles are those
910 defined in Fig. 3 and the cross symbols again show the imaginary refractive indices
911 necessary to reproduce the single-scattering albedo spectra inferred for the TC by
912 Tice et al. (2013). It was these properties that were assumed for the LTC here.

913

914

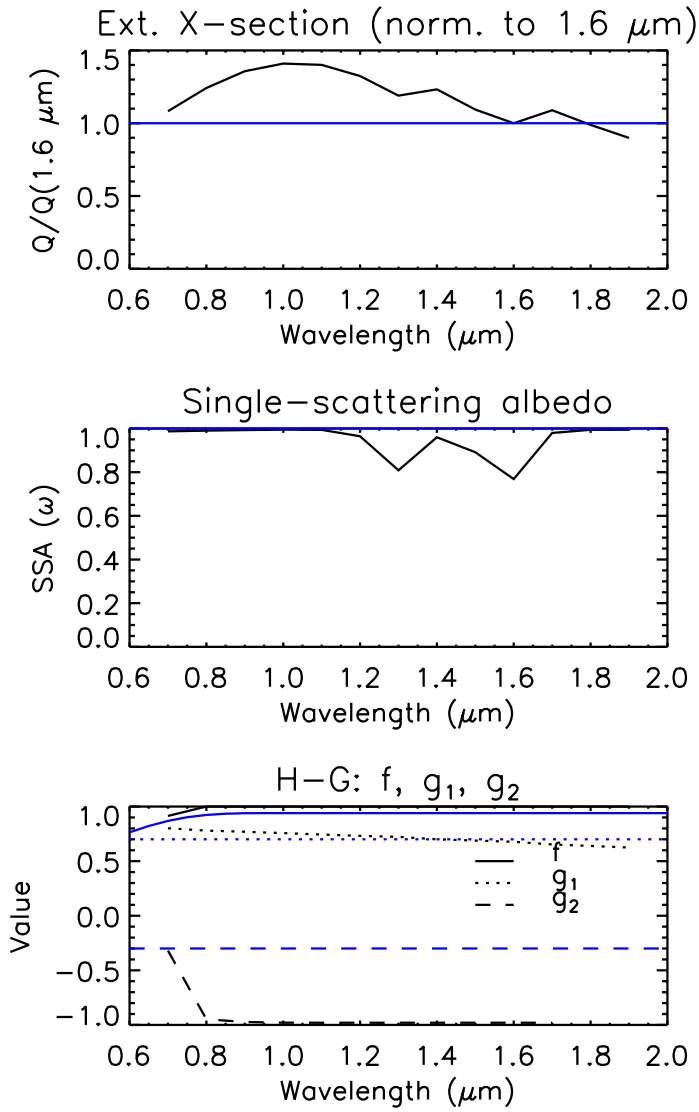

915

916 Figure 12. Retrieved scattering properties of the Middle Tropospheric Cloud (MTC)
917 using the 5-cloud SFK2011 model, with modified LTC properties, with a priori
918 imaginary refractive index set to 0.001±50%. The corresponding scattering properties
919 assumed by SFK2011 for tropospheric particles are marked in blue.

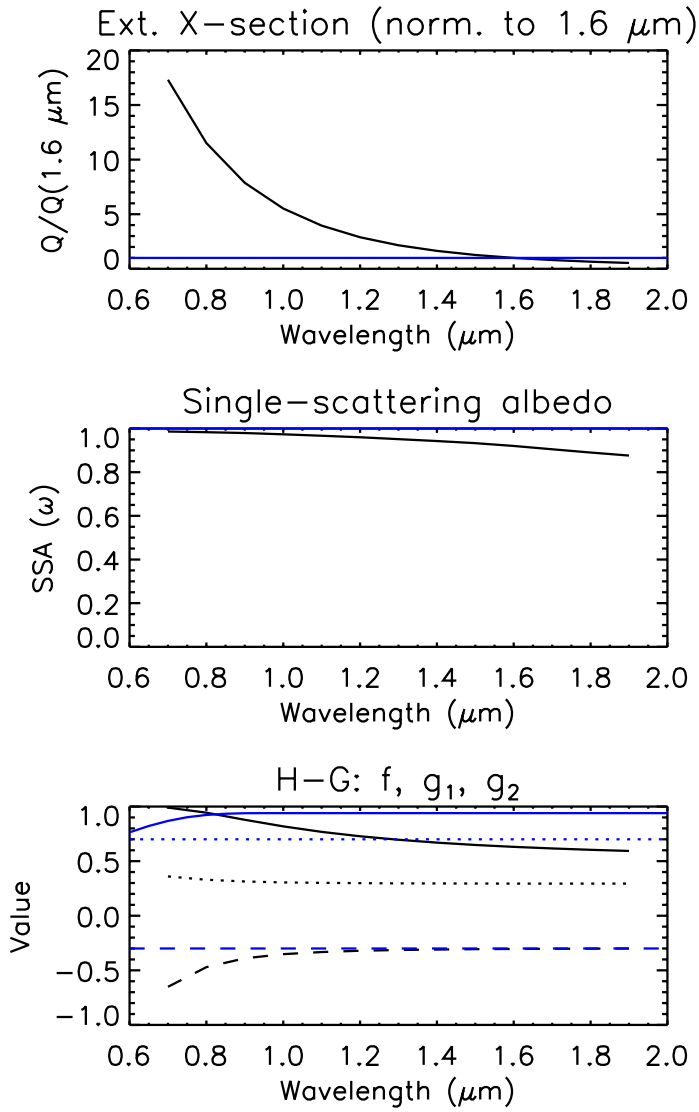

920

921 Figure 13. Retrieved scattering properties of the Tropospheric Haze (TH) using the
922 modifed 5-cloud SFK2011 model, with revised LTC properties, with a priori
923 imaginary refractive index set to 0.001±50%. The scattering properties assumed by
924 SFK2011 for tropospheric particles are marked in blue.

925

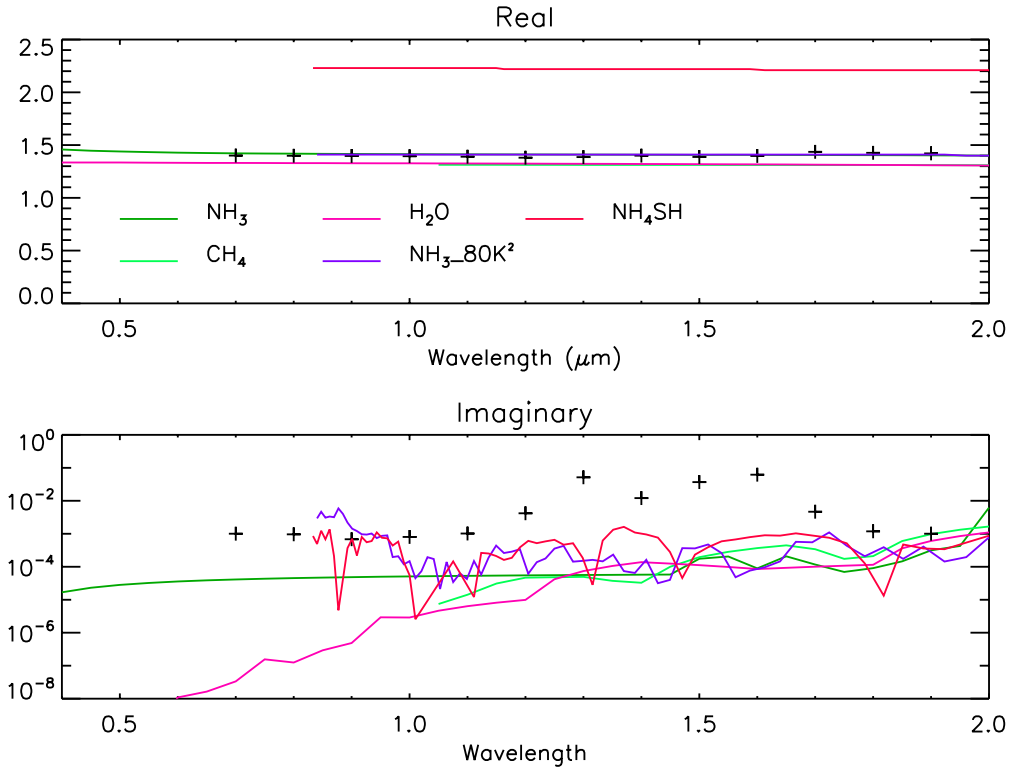

926

927 Figure 14. Comparison of retrieved tropospheric cloud (TC) refractive indices (for
928 self-consistent 2-cloud model) with published literature referred to in the text. There
929 are two sources of NH_3 data, with the data from Howett et al. (2007) indicated by the
930 ^{2}superscript. The retrieved TC refractive indices are indicated by the cross symbols.

931